velocity and slurry concentration. The holdup increases monotonically with increase in nitrogen velocity indicating the absence of foaming and strong liquid circulation patterns. The slurry concentration effect is negligibly small for 19.0 and 50.8 mm probes. For 31.8 mm probe, an increase in slurry concentration decreased the holdup. For this probe in Fig. 4.16, we have attempted to highlight the influence of particle diameter in the slurry on holdup. We conclude on the basis of these two figures, that nitrogen holdup is independent of slurry concentration and powder particle diameter in the slurry. In both these figures, the continuous curves are the smooth plots representing the most probable values. In Fig. 4.17, these data are plotted for 36.6 μm powder slurries at four concentrations to highlight the effect of probe diameter which is found to be sufficiently weak. Smoothed nitrogen holdup values are reported in Table 4.4.

4.4 Heat Transfer Data for Small Column

Experimental heat transfer studies were carried out in semi-batch mode for two- and three-phase systems at ambient conditions. Some heat transfer data are taken in the continuous mode also to establish the influence of liquid velocity on h_W. The heat transfer surfaces employed include three single tubes of different diameters, a five-, and a seven-tube bundle. The variation of h_W with location is also established for a given internal.

4.4.1 Operating Mode and a Typical Procedure

A series of measurements are taken to establish the experimental methodology for measuring heat transfer probe surface and the surrounding air-water dispersion. h_W is computed from the knowledge of the heat flux, Q, surface area of the probe, A, and the temperature difference between average probe surface, T_S , and average bulk temperature of the dispersion, T_C , on the basis of the following equation:

$$Q = h_W A (T_S - T_C) = I.V \qquad 4.10$$

To establish T_C accurately, radial temperature profiles are measured

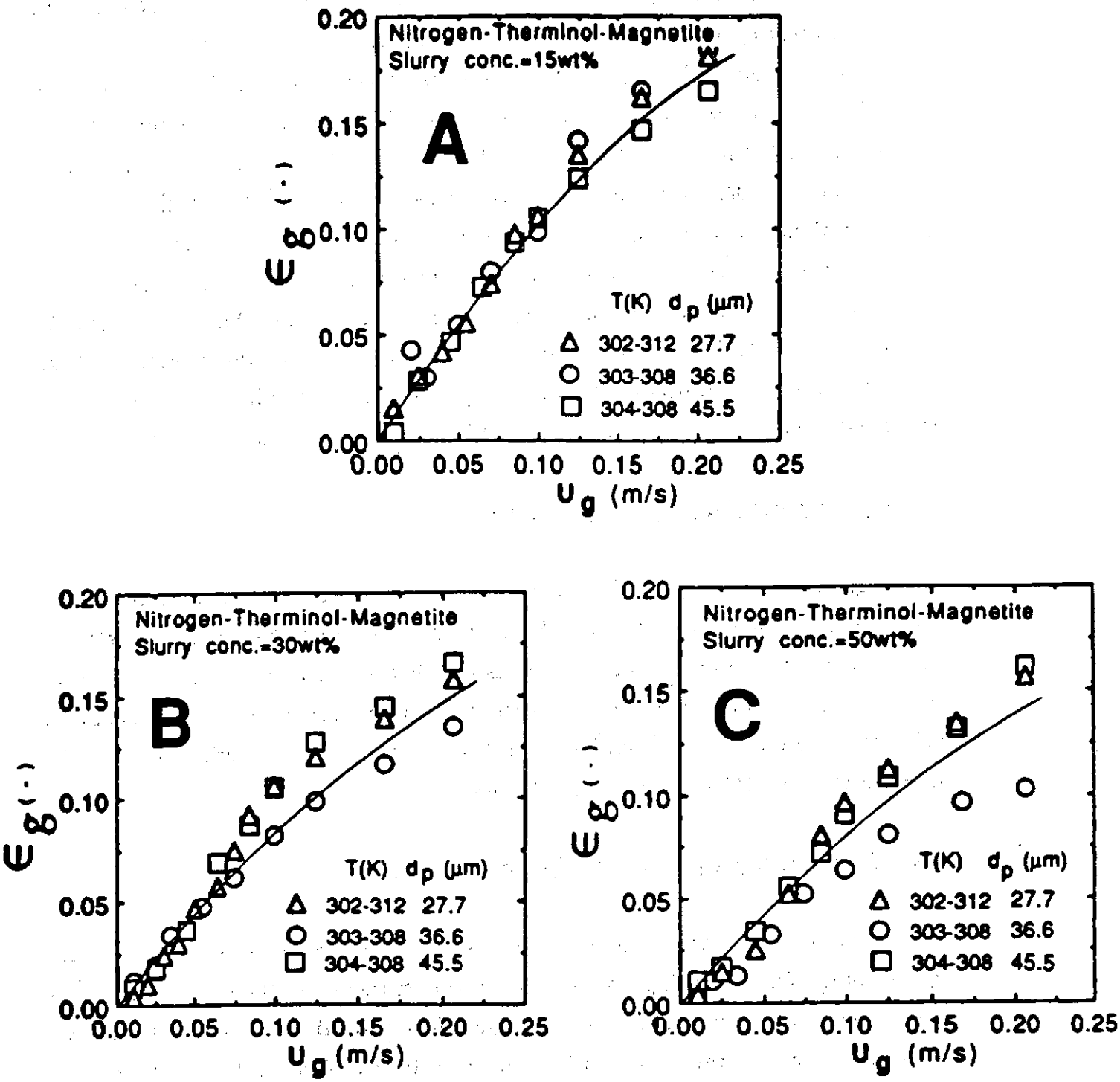

Fig. 4.16. Effect of particle diameter on nitrogen holdup for the 31.8 mm probe internal at solids concentration in weight percent of (A): 15, (B): 30, and (C): 50.

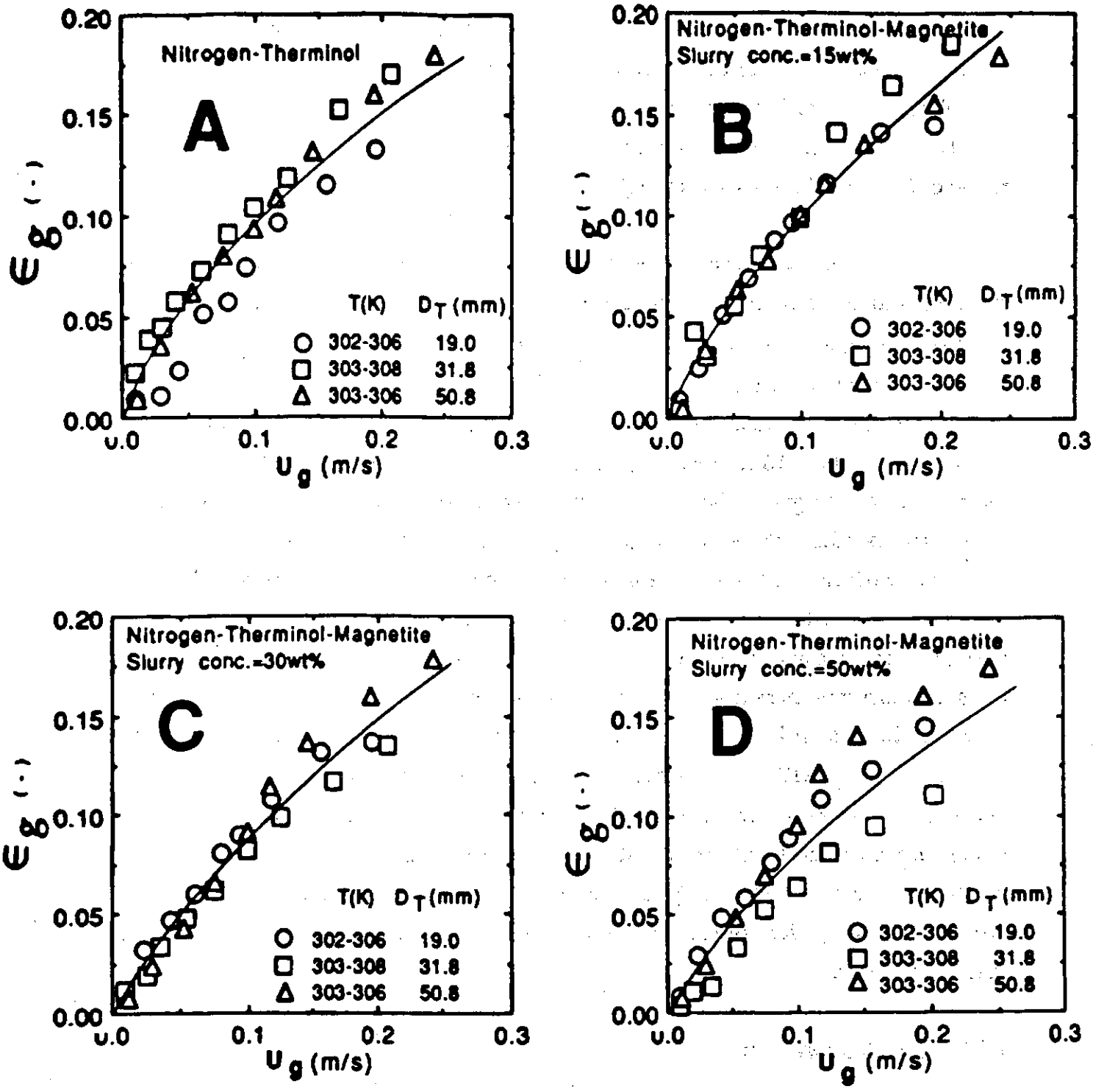

Fig. 4.17. Effect of probe diameter on nitrogen holdup at different solids concentrations in weight percent of (A): 0, (B): 15, (C): 30, and (D): 50.

corresponding to the midpoint of the heat transfer probe surface and at several radial locations. T_c is given by the arithmetic mean of the temperature values on the flat portion of the profile of the plot of temperature versus radial distance. A typical plot of radial temperature profiles measured at distances of 0.5 to 44.5 mm from the heat transfer probe surface and in the dispersion temperature range of 316 - 325 K is shown in Fig. 4.18.

The column temperature is found fairly uniform all along the radial distance and the degree of variation is dependent on the air velocity when it is less than 0.1 m/s. The variation in radial temperature is $\pm$ 0.4°C for $U_g < 0.1$ m/s and $\pm$ 0.2°C for $U_g > 0.1$ m/s.

Experiments are also conducted to investigate the dependence of h_w on heat flux.(Q = 468, 607, 813 and 943 W) in the air velocity range 0.04 to 0.42 m/s and the h_w values are given Table 4.12. These measurements revealed that h_w to be almost independent of the heat flux. h_w varies by about 1.2% only.

The variation of heat transfer coefficient with time is established to ascertain the steady state conditions in the column at a given gas velocity. Such variations are shown in Fig. 4.19. It is clear that the steady state sets in early as the gas velocity is increased. The steady state conditions are established typically between 10 - 20 min in the present studies. It is also established that the variation of h_w with time remained the same for continuous operating mode and the results are shown in Fig. 4.20. After these preliminary investigations h_w values are measured only under steady state conditions. Once the steady state conditions are attained at a given gas velocity, ten instantaneous values of h_w are calculated by the computer on-line and the h_w is taken to be the mean of these ten values.

4.4.2 Air - Water system

Heat transfer data measured in the 0.108 m bubble column between immersed surfaces and the surrounding air - water dispersion in semi-batch mode and for decreasing air velocities are presented in this section.

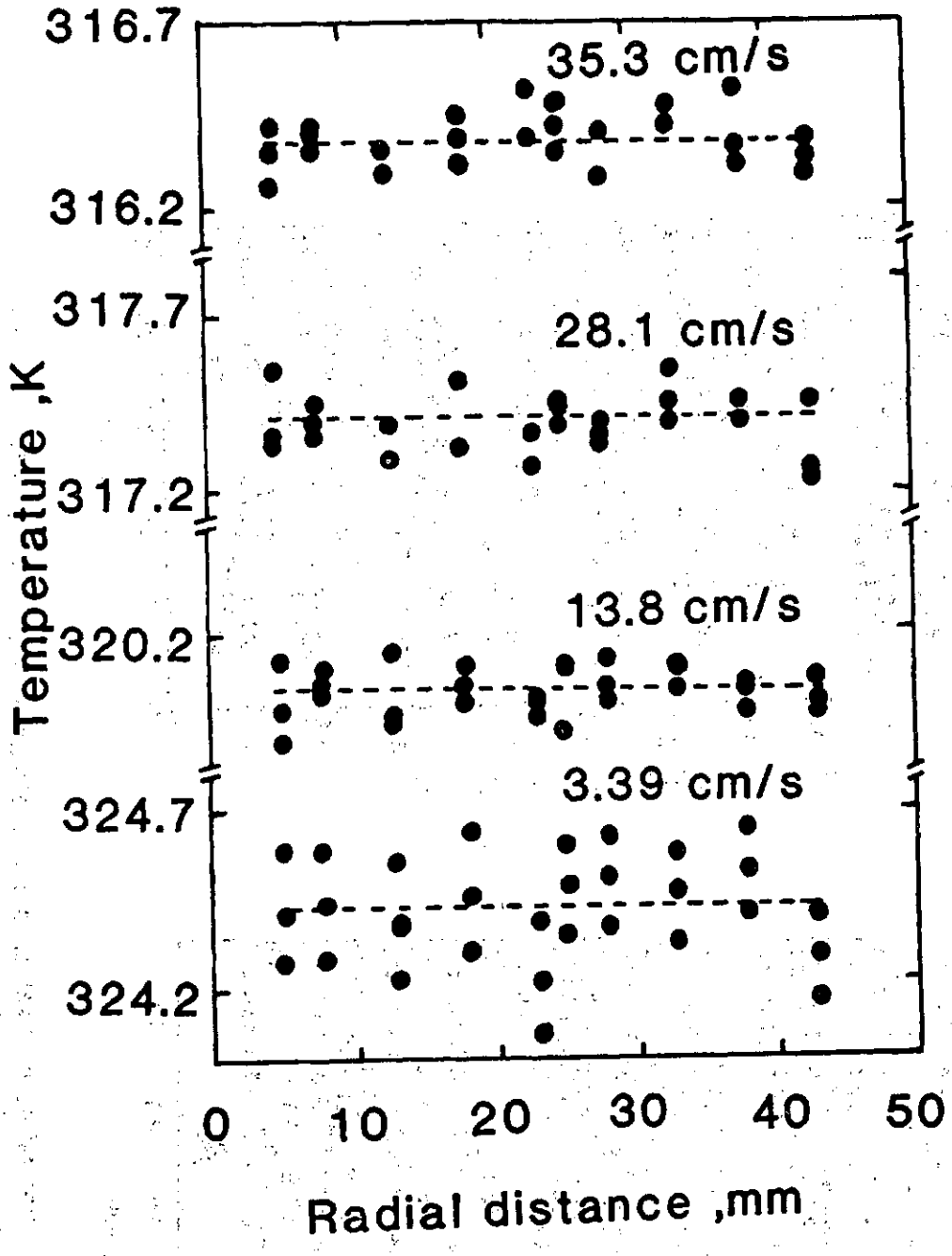

Fig. 4.18. Variation of column temperature as a function of radial distance from the probe surface at various air velocities.

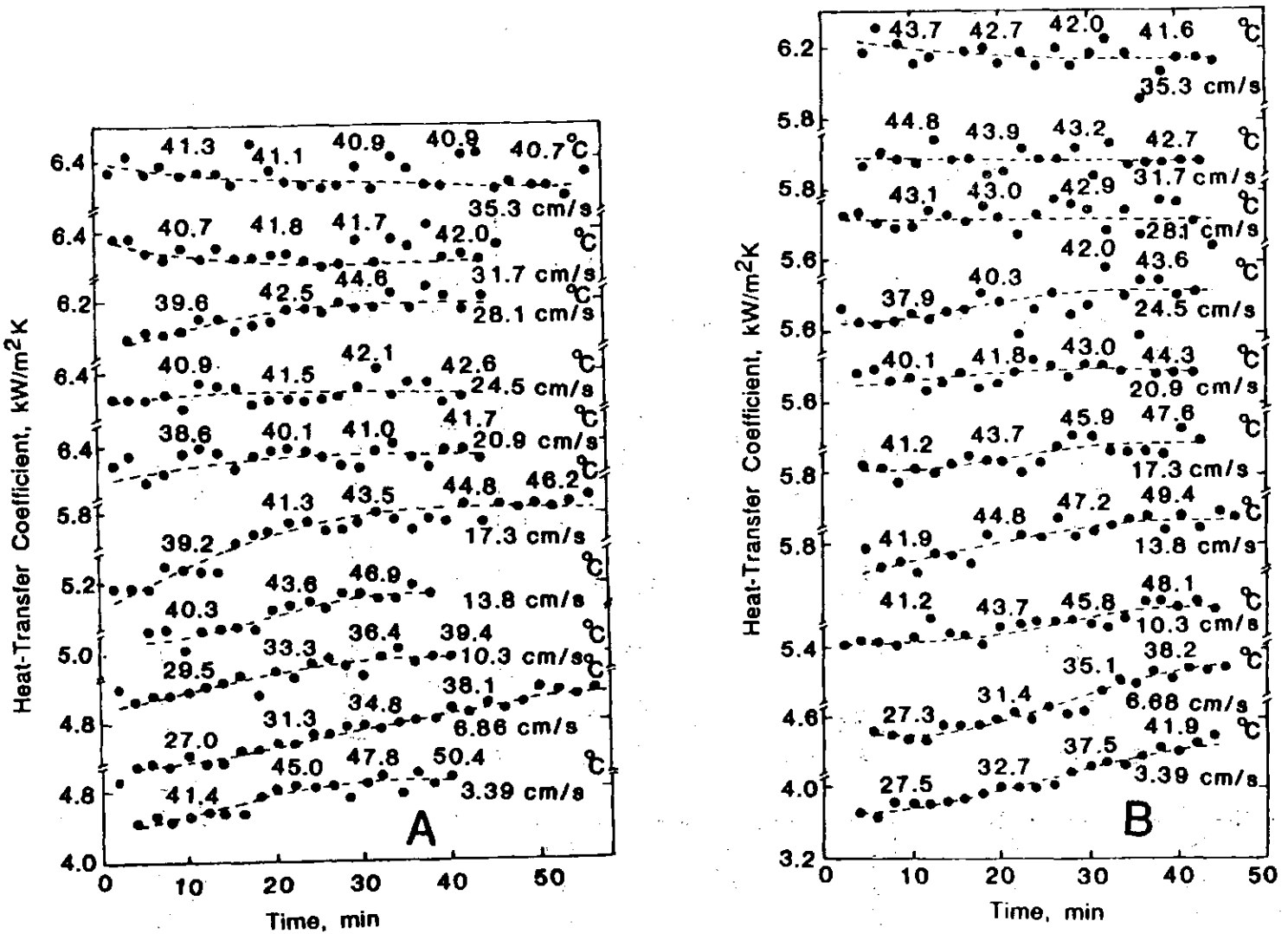

Fig. 4.19. Variation of heat transfer coefficient with time at different air velocities at two different locations in the column: (A) 0.57m, and (B) 1.18m above the distributor plate.

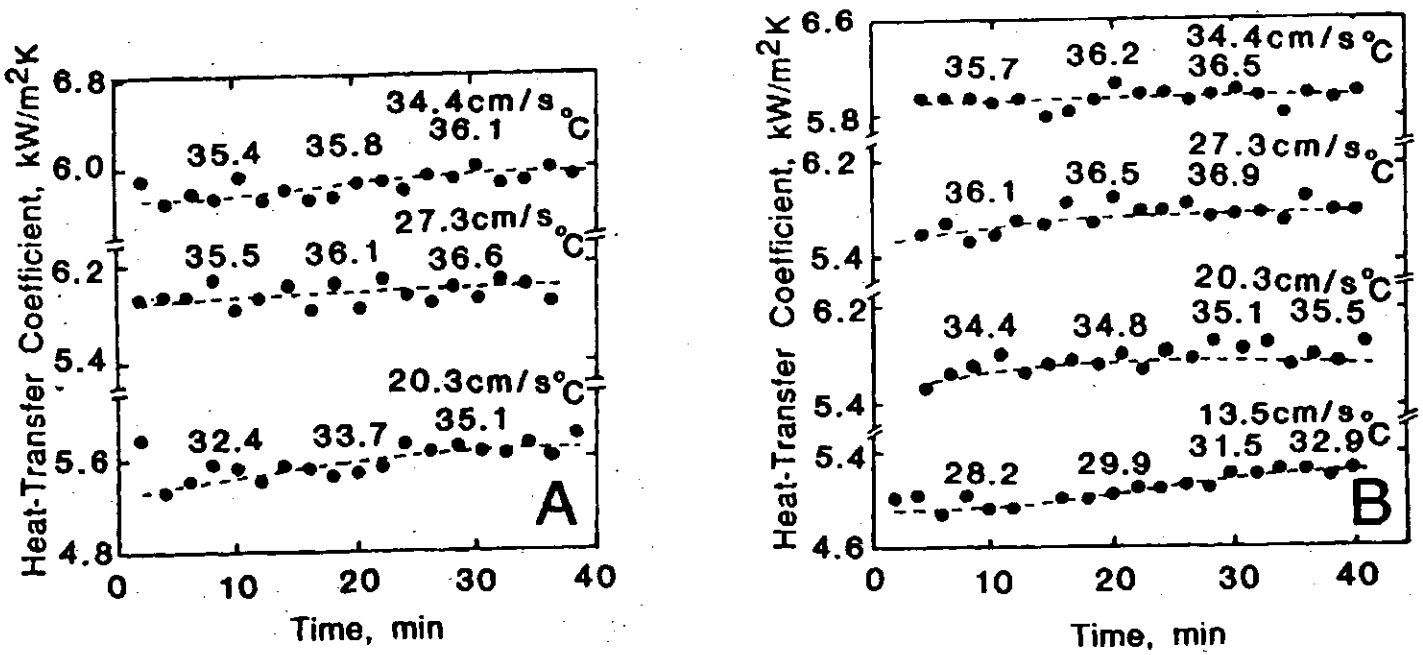

Fig. 4.20. Variation of the heat transfer coefficient with time at different air velocity for the water flow rate of 6.8 mm/s (A), and 11.9 mm/s (B).

Table 4.12. Experimental values of h_W (kW/m^2K) for different electrical power inputs to the heater at a fixed column temperature T_c. Column diameter: 0.108m, Internal: 19 mm single tube. System: Air-water.

T_c (K)	Q (W)	h_W (kW/m^2 K)
312.7 ± 0.8	468	5.915 ± 0.089
312.6 ± 0.6	670	5.779 ± 0.216
313.8 ± 1.1	813	5.937 ± 0.082
312.0 ± 1.4	943	6.003 ± 0.340

Table 4.13. Experimental h_W (kW/m^2K) and air holdup values for air-water system in the continuous mode operation at 307±1K. Column diameter: 0.108 m, Internal: 19 mm single tube.

U_g (m/s)	V_L (cm/s)= 0.0		V_L (cm/s)= 6.8		V_L (cm/s)= 11.9	
	h_W	ϵ_g	h_W	ϵ_g	h_W	ϵ_g
0.135	5.31	0.202	-	-	5.22	0.233
0.203	5.62	0.240	5.64	0.305	5.76	0.295
0.273	5.79	0.301	5.96	0.338	5.72	0.336
0.344	5.72	0.339	5.92	0.379	5.88	0.361

4.4.2a Effect of the Location of Heat Transfer Surfaces

The 19 mm diameter heat transfer probe is axially placed and has three individual heat transfer surfaces whose midpoints are located at 0.522, 0.875 and 1.181 m above the gas distributor plate. The steady state h_w values measured at these three locations in the column (lower, middle and upper regions) are presented in Fig. 4.21 and in Table 4.14. It is seen from this plot that h_w values increase with an increase in U_g (U_g < 0.15 m/s) initially and attain a constant value for U_g > 0.15 m/s. The variation of h_w with location of heater surface is negligibly small.

Similar heat transfer data for the 19mm diameter heat transfer probe are measured in the middle region. Four sets of data obtained are presented later in Fig. 6.2 and given in Table 4.15A. Smoothed h_w values based on the above measurements are given in Table 4.15B.

Similar heat transfer data are measured at three heater locations in a seven-tube bundle and are presented in Fig. 4.22. The influence of slumped liquid height (or dispersion height) on h_w for the axially located middle heater is shown in Fig. 4.23.

The results indicate that h_w is smaller in the bottom region of the column compared to the middle and upper regions. The variation in h_w values could be due to different circulation patterns that may exist in the upper and lower regions of the column which represent varying degrees of liquid circulation. A comparison of h_w values for a single tube and seven-tube bundle in the middle region indicate that the influence of neighboring tubes is to enhance h_w. The experimental h_w values are given in Table 4.16.

4.4.2b Effect of liquid velocity

A series of experiments is conducted to establish the influence of continuous phase (water) flow rate on h_w. The conditions were similar as described above and the liquid velocity was varied up to 11.9 mm/s. The h_w values at 307K are presented in Fig. 4.24. The influence of liquid velocity in the

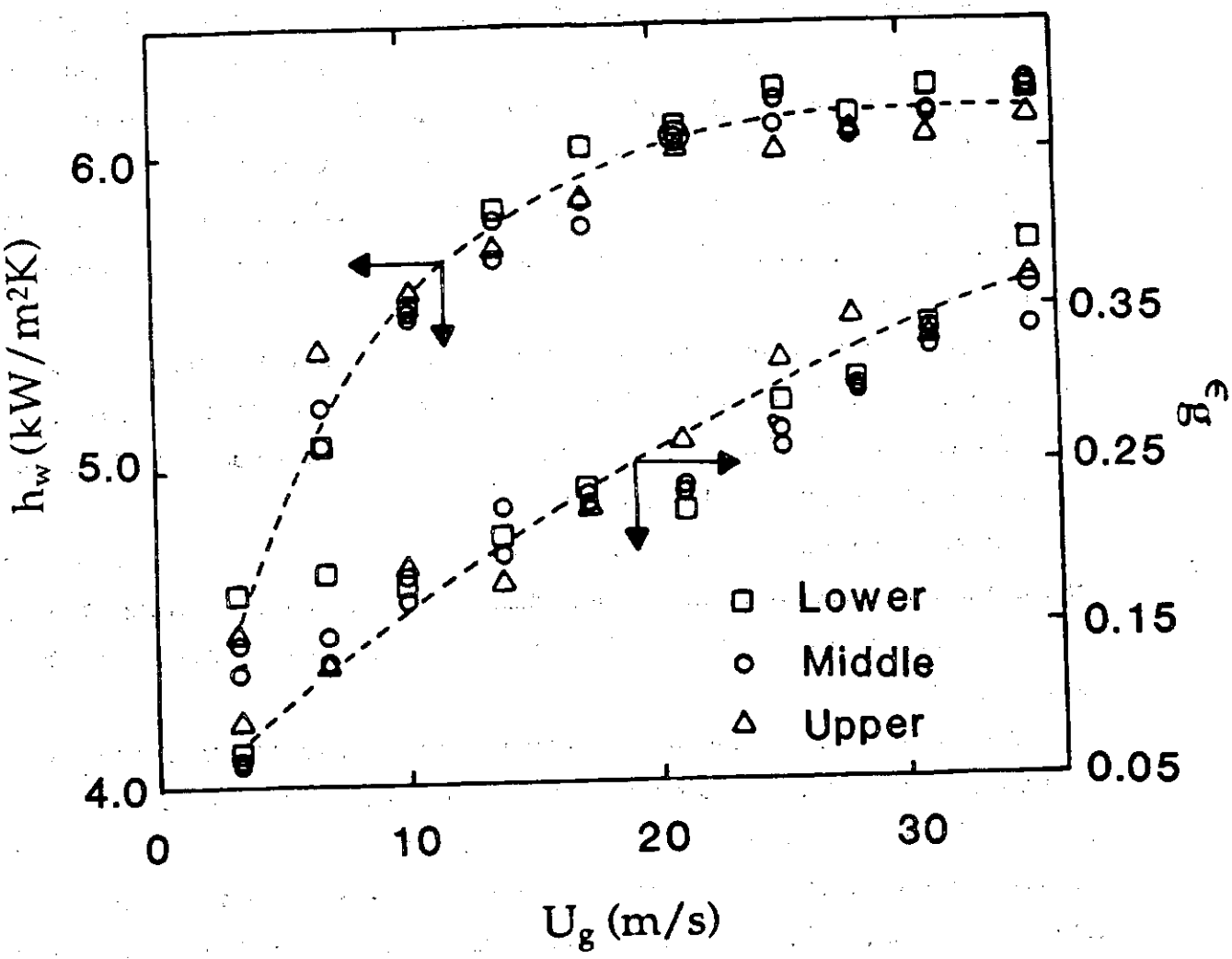

Fig. 4.21. Variation of the heat transfer coefficient and average air holdup as a function of air velocity for three heater locations in the column.

Table 4.14. Experimental h_W (kW/m^2K) and air holdup values at different heater locations for air-water system at 315± 1 K. Column diameter: 0.108 m, Internal: Seven-tube bundle.

Air Velocity, V	Lower (H = 57.2 cm)		Middle (H = 87.5 cm)		Middle (H = 87.5cm)		Upper (H = 118.1 cm)	
cm/s	h_W, kw/m^2K	ϵ_g	h_W, kw/m^2K	ϵ_g	h_W, kw/m^2K	ϵ_g	h_W, kw/m^2K	ϵ_g
3.39	4.62	0.074	4.36	0.071	4.45	0.071	4.48	0.088
6.86	5.08	0.190	5.08	0.148	5.20	0.138	5.38	0.131
10.3	5.56	0.181	5.52	0.173	5.51	0.184	5.56	0.193
13.8	5.82	0.212	5.80	0.202	5.66	0.231	5.70	0.180
17.3	6.02	0.241	5.77	0.224	5.78	0.237	5.86	0.229
20.9	6.08	0.224	6.01	0.240	6.01	0.261	6.00	0.274
24.5	6.20	0.294	6.18	0.262	6.18	0.276	6.08	0.320
28.1	6.12	0.306	6.04	0.301	6.05	0.307	6.05	0.346
31.7	6.20	0.340	6.12	0.336	6.12	0.331	6.04	0.337
35.3	6.18	0.397	6.20	0.339	6.19	0.394	6.10	0.372

Table 4.15. Experimental (A) and smoothed (B) h_W (kW/m^{2}K) values for air-water system at 309K. Column diameter: 0.108 m, Internal: 19 mm single tube.

A

SET - 1		SET - 2		SET - 3	
U_g (m/s)	h_w (kW/m^{2}K)	U_g (m/s)	h_w (kW/m^{2}K)	U_g (m/s)	h_w (kW/m^{2}K)
0.0086	2.77	0.0130	2.80	0.033	4.11
0.0170	3.10	0.0215	3.27	0.066	4.72
0.0258	3.66	0.0301	3.67	0.099	5.17
0.0344	4.19	0.0344	3.90	0.132	5.37
0.0430	4.30	0.0387	4.15	0.166	5.42
0.0473	4.64	0.0430	4.30	0.199	5.70
0.0516	4.52	0.0473	4.36	0.233	5.71
0.0560	4.54	0.0560	4.52	0.266	5.80
0.0602	4.72	0.0645	4.74	0.300	5.87
0.0645	4.72	0.0688	4.75	0.333	5.79
0.0688	4.77	0.0730	4.82		
0.0730	4.98	0.0774	4.84	SET - 4	
0.0817	4.85	0.0817	4.84		
0.0860	4.95	0.0832	5.09	0.0086	2.45
0.116	5.33	0.099	5.25	0.0130	2.85
0.148	5.34	0.115	5.42	0.0258	3.80
0.181	5.50	0.132	5.58	0.0301	3.98
0.214	5.70	0.148	5.66	0.0387	4.34
0.247	5.78	0.181	5.75	0.0430	4.56
0.281	5.77	0.214	5.75		
0.313	5.59	0.247	5.85		
0.333	5.48	0.281	5.71		
		0.313	5.82		

B

U_g	h_w	U_g	h_w	U_g	h_w
0.009	2.66	0.045	4.47	0.085	4.98
0.012	2.82	0.050	4.58	0.090	5.02
0.015	2.96	0.055	4.67	0.095	5.08
0.020	3.24	0.060	4.72	0.10	5.12
0.025	3.57	0.065	4.77	0.15	5.50
0.030	3.86	0.070	4.80	0.20	5.68
0.035	4.08	0.075	4.86	0.25	5.76
0.040	4.28	0.080	4.92	0.30	5.78
				0.33	5.77

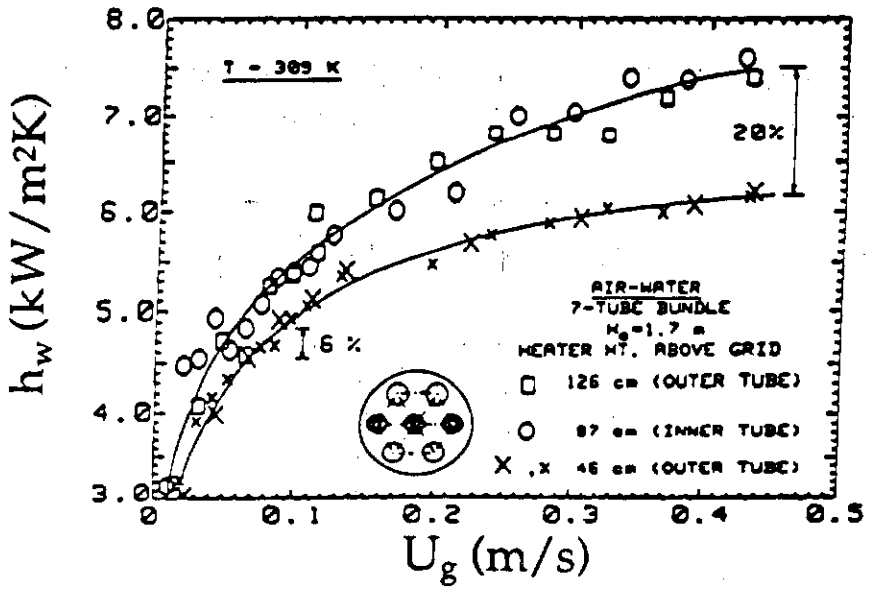

Fig. 4.22. Dependence of heat transfer coefficient for the central tube in the bundle on air velocity.

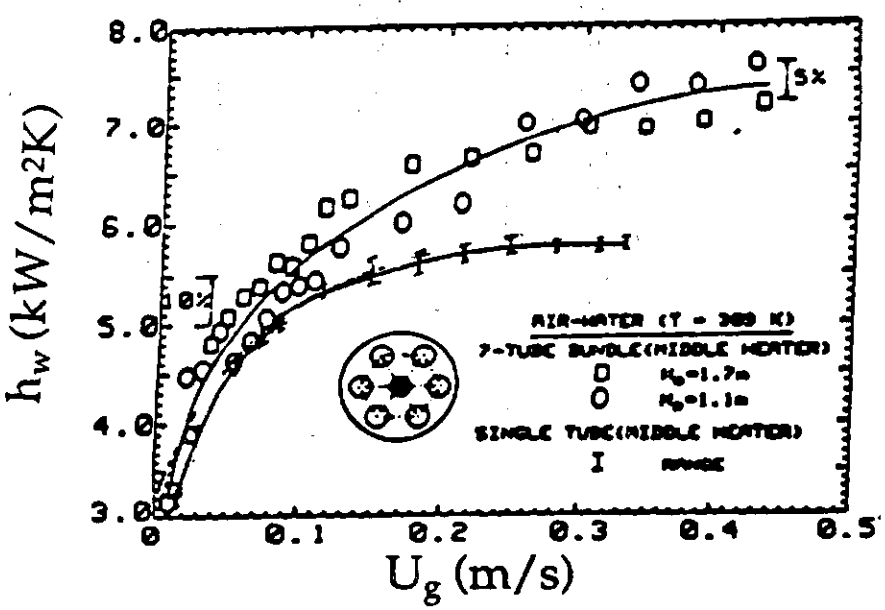

Fig. 4.23. Dependence of heat transfer coefficient on heater location in the bundle and air velocity.

Table 4.16. Experimental h_w (kW/m^2K) values for air-water system at 309K. Column diameter: 0.108m, Internal: Seven-tube bundle.

U_g (m/s)	h_w (kW/m^2K)
0.011	3.14
0.022	4.46
0.033	4.53
0.044	4.92
0.055	4.61
0.066	4.82
0.077	5.05
0.088	5.32
0.099	5.38
0.110	5.43
0.126	5.25
0.169	5.99
0.212	6.17
0.256	6.99
0.298	7.03
0.340	7.35
0.383	7.37
0.426	7.59

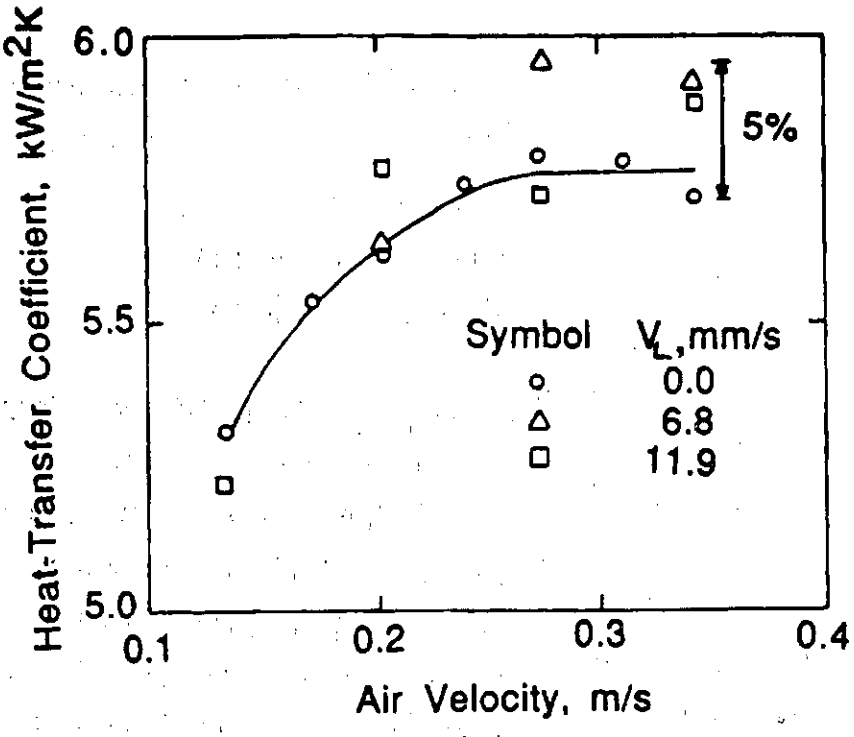

Fig. 4.24. Variation of the heat transfer coefficient at 307K with air velocity at different water flow velocities.

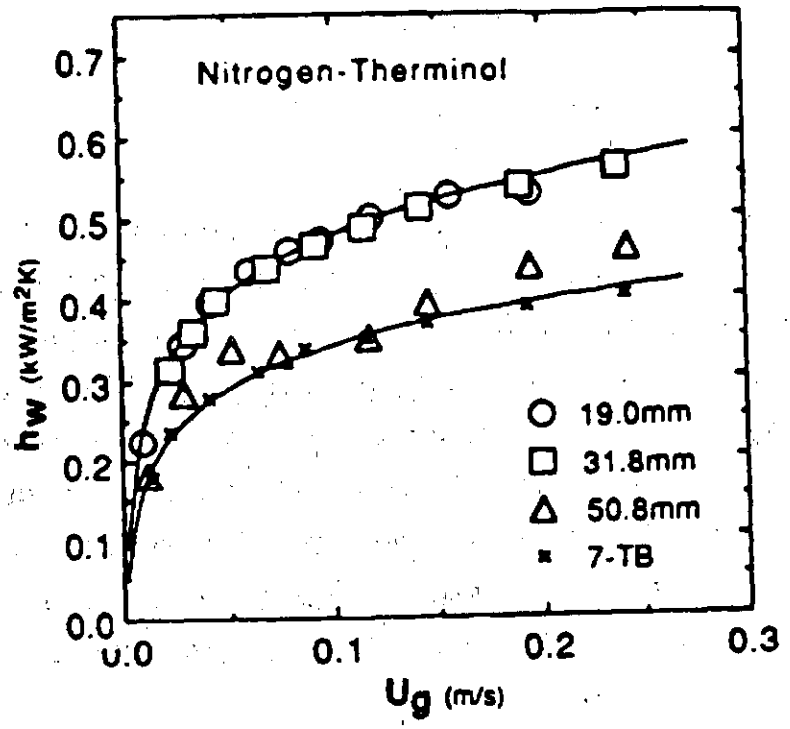

Fig. 4.25. Dependence of heat transfer coefficient on the nature of internals in the column.

present experiments seems to be negligibly small as the scatter is always within the experiment uncertainty of ±5 percent. The experimental h_W values are listed in Table 4.13.

4.4.3 Nitrogen - Therminol system

The influence of internals on h_W is investigated for nitrogen-Therminol system with three different size single tubes and with a seven-tube bundle. The h_W results are presented in Fig. 4.25 and these indicate that h_W increases rapidly with increase in nitrogen velocity up to 0.1 m/s and almost approaches a constant value thereafter for all internals. The dependence of h_W on the geometry of internals appears to be involved and it is interesting to note that the two internals (single tube, 50.8 mm; and the seven-tube bundle) having the same blockage area in the column but different geometry exhibit similar influence on h_W. On the otherhand, the smaller size internals (19.0 and 31.8 mm) having lower but different blockage areas have similar h_W values. The smoothed h_W data are given later in Table 4.21.

4.4.4. Air-Water-Red Iron Oxide System

Heat transfer data are measured for the air-water-red iron oxide system in the 0.108 m column equipped with a 19 mm single probe and the experiments are conducted in the semi-batch mode. The h_W values are plotted as a function of air velocity at a constant temperature of 313 K in Fig. 4.26. The two-phase and three-phase h_W values corresponding to the lowest concentration of solids are almost identical and hence only the latter results are shown in Fig. 4.26. The h_W values increase with air velocity and approach a constant value at higher air velocity values. At a given air velocity, h_W value decreases with increase in slurry solids concentration. These qualitative trends apply only to the range of variables covered in Fig. 4.26.

Results similar to those of Fig. 4.26 are displayed in Fig. 4.27 for red iron oxide powder of mean diameter 2.38 μm. The qualitative features of these data are the same as those of the powder of 1.02 μm. These results are also in

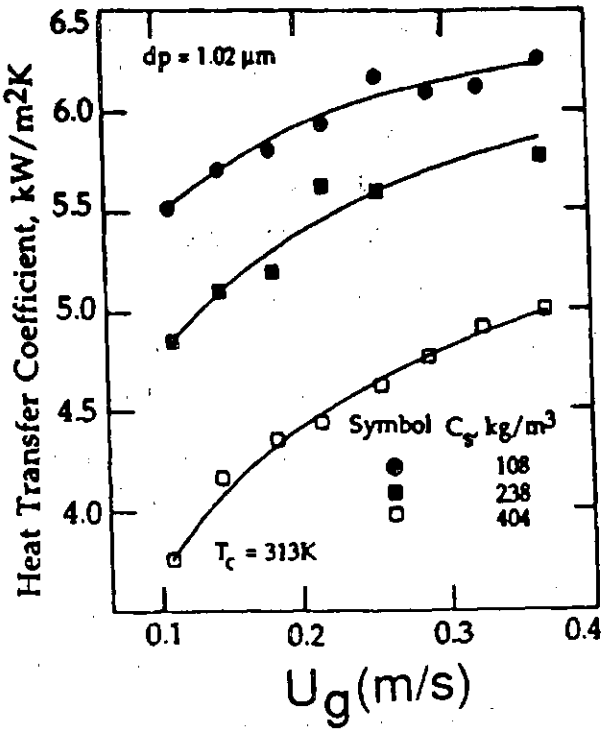

Fig. 4.26. Variation of heat transfer coefficient with air velocity at three concentrations of slurry of 1.02 μm mean iron oxide particles in water at 313K.

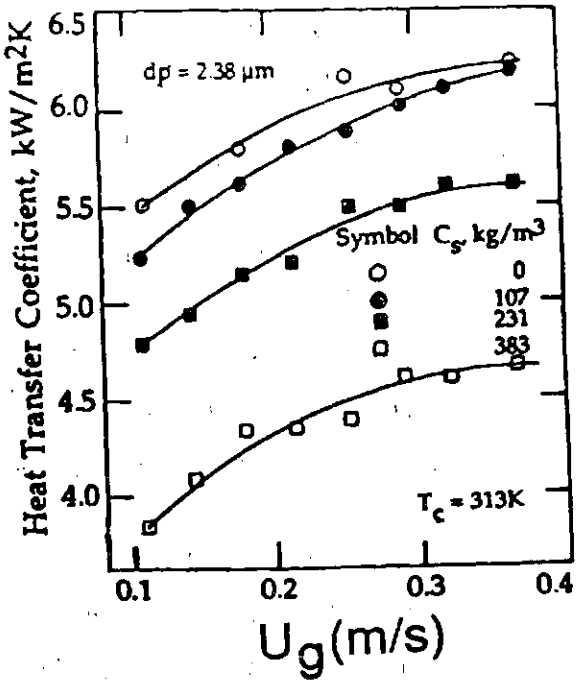

Fig. 4.27. Variation of heat transfer coefficient with air velocity at three concentrations of slurry of 2.38 μm mean iron oxide particles in water at 313K.

complete accord with the results of Fig. 4.26 and follow the same qualitative trends of variation in relation to air velocity and slurry concentration. The experimental h_w values are presented in Table 4.17.

Similar data are obtained with a seven-tube bundle in the semi-batch mode for decreasing air velocity [130]. The measured heat transfer coefficient values for the central innermost tube in the bundle are graphically displayed in Fig. 4.28 as a function of air velocity. Concentrations of iron-oxide (mean particle diameter 1.02 and 2.38 μm) in water having the values of 0, 5, 10, and 20 weight percent in the slurry have been investigated. Repetitive runs have been made for the air-water system and the shaded area in Fig. 4.28 represents the range of maximum variation. The continuous curve is a smooth plot through the experimental points. This figure clearly demonstrates two interesting qualitative results. First, h_w increases with increase in air velocity for both two- and three-phase systems. The increase is rapid in the beginning but slows down as the air velocity is increased. Secondly, the h_w values do not significantly change with the addition of iron-oxide in water, but as the concentration of the powder increases in the slurry the h_w values decrease at a given air velocity, U_g. The most concentrated slurry for 1.02 μm powder has h_w values which are about 6 percent smaller than the corresponding two-phase values at higher air velocities. The data for 2.38 μm size powder slurries (0, 5, and 10 wt.%) show negligible influence of slurry concentration on h_w.

In Fig. 4.29A, these data are displayed to highlight the influence of particle size, d_p, on h_w for relatively dilute dispersions. No effect on h_w is evident. This is understandable when it is recalled that heat removal occurs via liquid or slurry elements and the rheology of such dispersions is not likely to be influenced appreciably by changes of the solid phase properties by as small amounts as involved here.

Lastly in Fig. 4.29B, h_w values for the tube bundle are compared with the single tube values for otherwise under identical conditions for the slurries of two powders. It is interesting to note that the tube bundle configuration leads to h_w values which are about ten percent larger than the corresponding single tube values. It appears that the bubble size is smaller and liquid mixing is better with

Table 4.17. Experimental h_W (kW/m^2K) values for air-water-red iron oxide and air-water-magnetite systems at 313K. Column diameter: 0.108 m, Internal: 19 mm single tube.

Slurry	$C_s \backslash U_g$	0.108	0.145	0.181	0.217	0.253	0.289	0.325	0.362
Iron Oxide	108	5.50	5.70	5.80	6.10	6.10	6.15	6.10	6.25
(d_p = 1.02 μm)	238	4.84	5.10	5.20	5.64	5.60	-	-	5.75
	404	3.75	4.15	4.40	4.43	4.60	4.75	4.93	5.02
Iron Oxide	107	5.25	5.50	5.60	5.80	5.85	6.00	6.10	6.20
(d_p = 2.38 μm)	231	4.80	4.95	5.15	5.20	5.50	5.50	5.60	5.60
	383	3.85	4.10	4.35	4.40	4.60	4.60	4.65	4.70
Magnetite	0	5.50	5.67	5.80	5.97	6.07	6.15	6.18	6.22
(d_p = 43.6 μm)	107	6.15	6.00	6.20	6.40	6.50	6.50	6.80	6.50
	167	5.70	6.00	6.25	6.50	6.45	6.50	6.75	7.20
	258	5.85	6.15	6.40	6.60	6.55	7.10	6.80	6.70

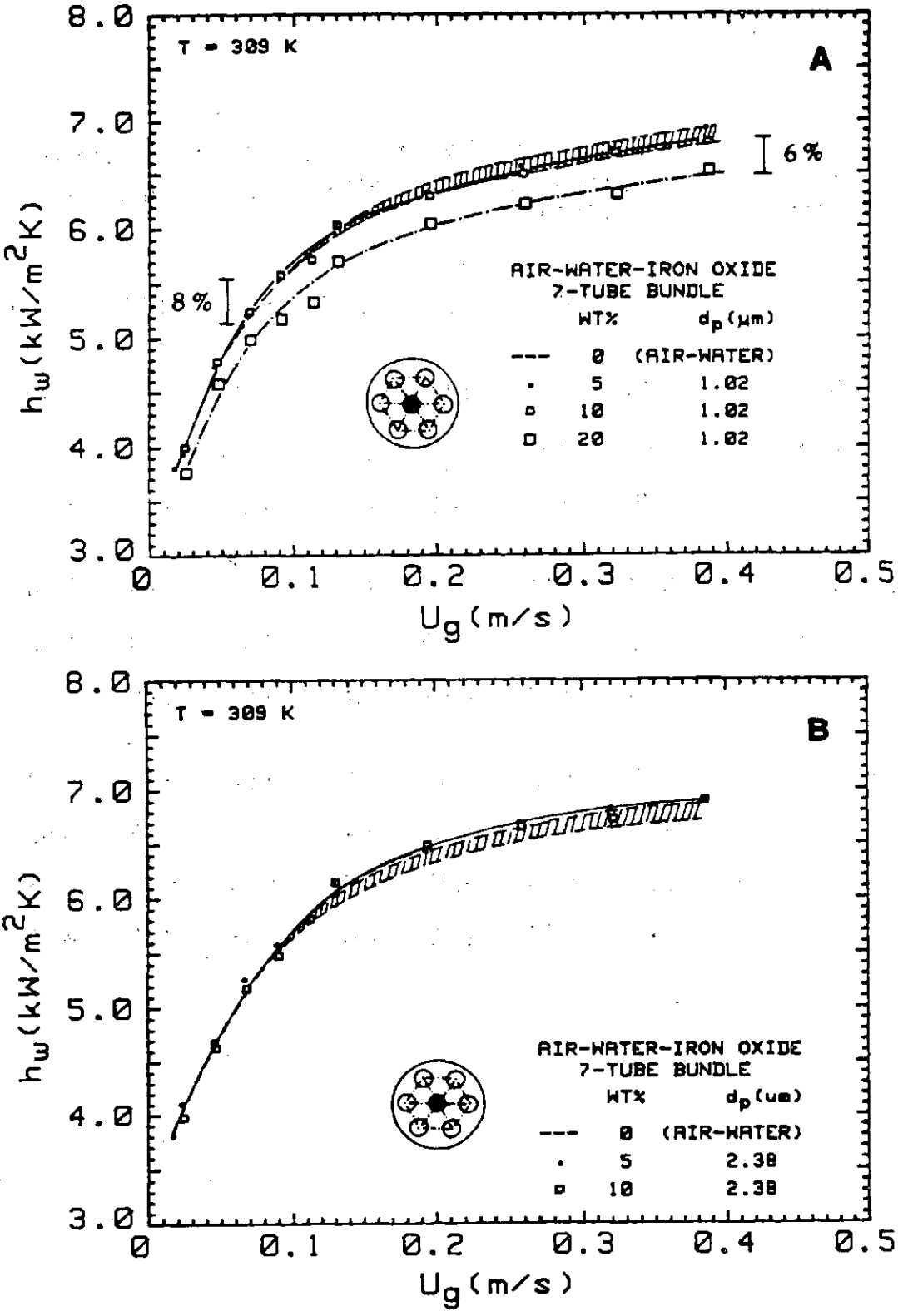

Fig. 4.28. Dependence of heat transfer coefficient on air velocity and solids concentration for particles of diameter (A) 1.02 μm, and (B) 2.38 μm, in the slurry.

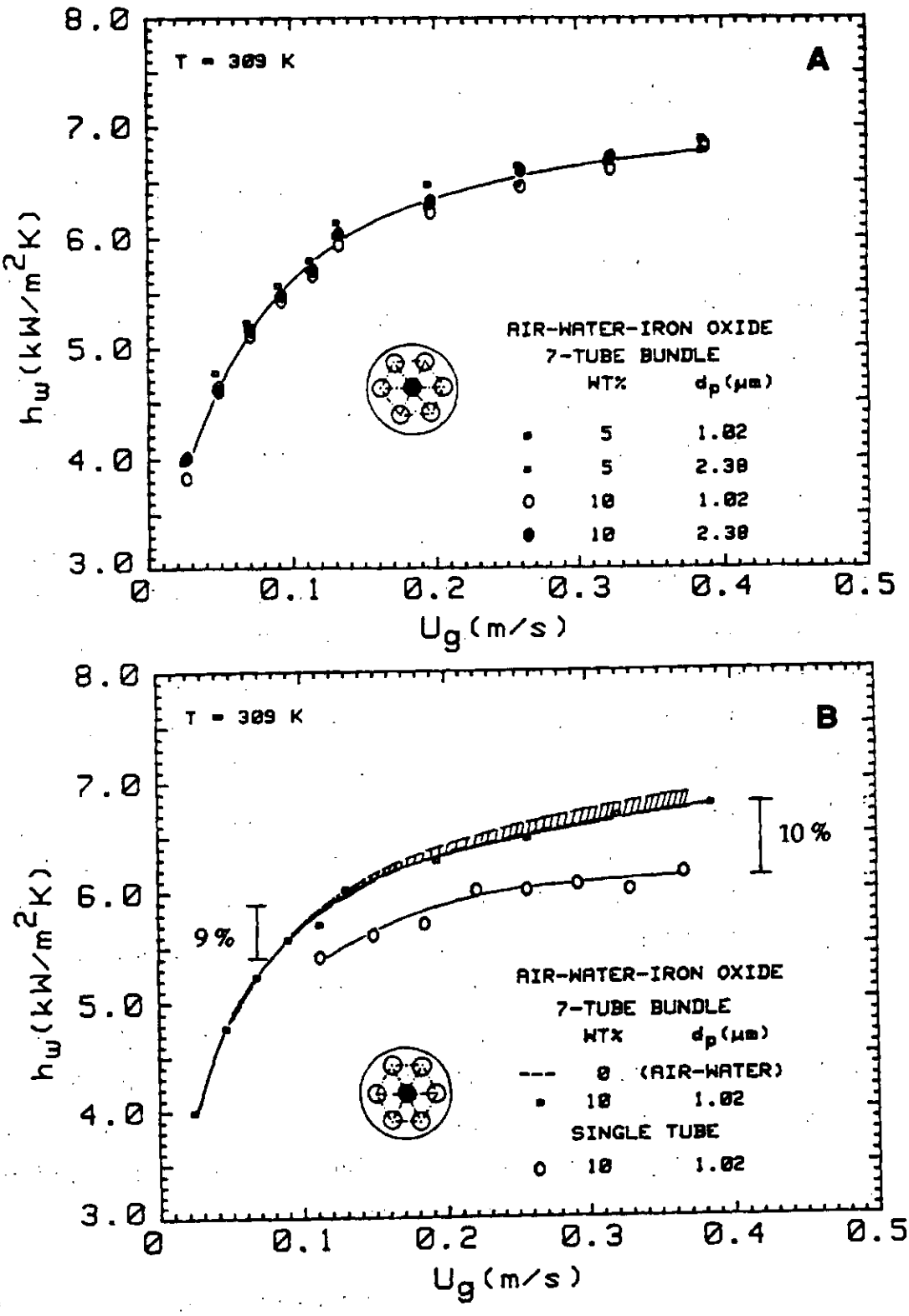

Fig. 4.29. Heat transfer coefficient dependence on (A) particle size and solids concentration in the slurry, and (B) nature of internals in the column.

the tube bundle in the column in comparison to the case when only a single probe is present.

4.4.5. Air-Water-Glass Bead System

Heat transfer coefficients between a 19 mm diameter vertical axially located probe and slurries of glass beads of different sizes (50.0, 117.6 and 143.3 μm) and concentrations (108-312 kg/m3) are measured in the semi-batch mode in the 0.108 m bubble column and are given in Table 4.18. The variation of h_w with air velocity and a slurry concentration of 0.104 kg/m^3 for 50.0 and 117.6 μm particles are shown in Fig. 4.30A and 4.30B respectively. The results indicate that h_w values for three phase systems are greater than for the corresponding two-phase system values.

h_w values are measured for three solids concentrations for d_p = 143.3 μm and C_s = 104, 214, and 312 kg/m^3 as a function of air velocity and are shown in Fig. 4.30C. The qualitative trends observed for the two other particles are further confirmed here. h_w values increase with an increase in air velocity and approach to a constant value as the air velocity is increased. At the same air velocity, h_w increases with an increase in solids concentration. The average increase over this velocity range, with an increase in C_s values is about 5.5, 8.5, 10.0 percent from the corresponding values for C_s = 0. It would thus appear that the increases in the C_s values cause only a small increase in the h_w values. These small increases in h_w values also suggest that probably the individual phases do not play an important role in altering the heat transfer rates. This is further discussed later.

The effect of d_p on h_w is explicitly displayed in Fig. 4.31 where the experimental data are plotted as a function of air velocity for all the three particles at a constant value of C_s = 104 kg/m^3 and T_c = 313-316 K. It is clear that the dependence of particle size on h_w in the size range investigated here (50.0 to 143.3 μm) is negligibly small when it is recalled that the estimated uncertainty of h_w values is about ± 4.5 percent.

A similar study with a seven-tube bundle revealed negligible influence of slurry concentration on h_w for a given particle size. The results are presented in Fig. 4.32. A cross plot of h_w as a function of U_g for different particle sizes at 10

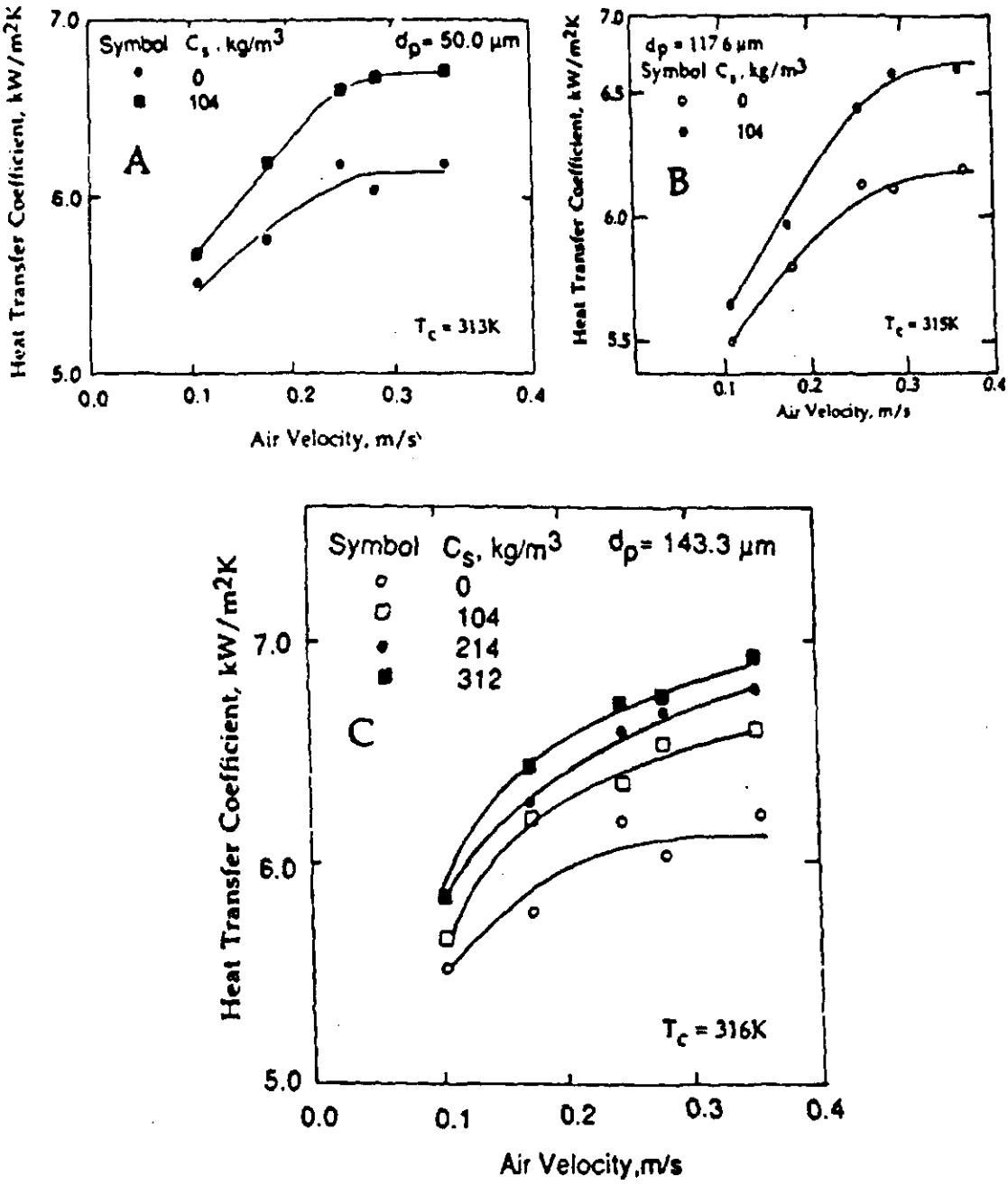

Fig. 4.30. Variation of heat transfer coefficient with superficial air velocity for slurries of different solids concentrations and particle size.

Table 4.18. Experimental h_w (kW/m^2K) values for air-water-glass bead system at 315K. Column diameter: 0.108m, Internal: 19mm single tube.

Air Velocity (m/s)	C_s (kg/m^3) =0	d_p=143.3 μm		
		C_s (kg/m^3) =104	=214	=312
0.103	5.52	5.66	5.84	5.84
0.173	5.77	6.20	6.28	6.44
0.245	6.18	6.36	6.60	6.72
0.281	6.04	6.53	6.68	6.76
0.353	6.20	6.60	6.78	6.92

Air Velocity (m/s)	d_p=50 μm		d_p=90 μm
	C_s (kg/m^3) =0	=108	=104
0.103	5.52	5.68	5.65
0.173	5.77	6.20	5.95
0.245	6.18	6.60	6.45
0.281	6.04	6.68	6.60
0.353	6.20	6.72	6.60

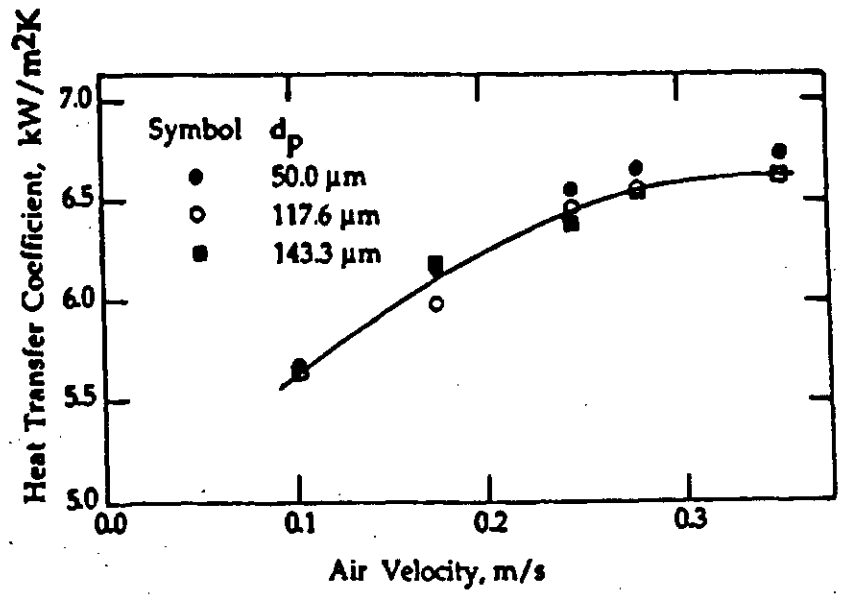

Fig. 4.31. Variation of heat transfer coefficient with superficial air velocity for slurries of different particle sizes at the solid concentration of 104 kg/m^3.

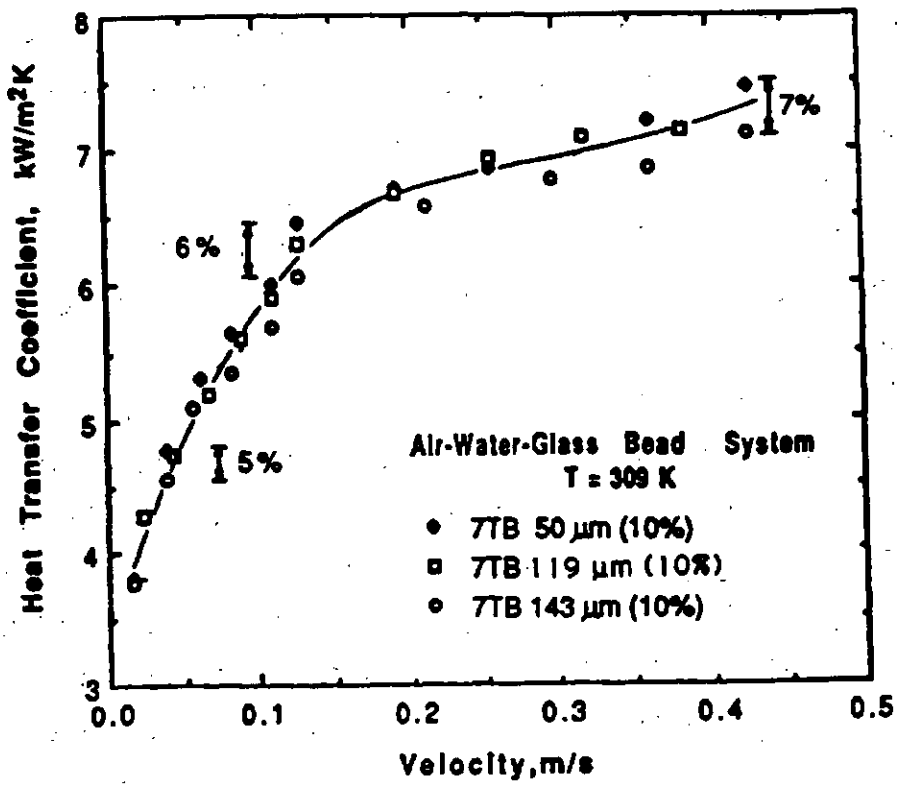

Fig. 4.33. Dependence of heat transfer coefficient on air velocity and particle diameter in the slurry.

wt.% solids concentration is shown in Fig. 4.33. It is of interest to note that particle size has negligible influence on h_w for a seven-tube bundle and this result is similar to that observed for a single tube (Fig. 4.31). The smoothed h_w data are given in Table 4.19.

4.4.6 Air-Water-Magnetite System

A more exhaustive study of heat transfer is conducted with a 19 mm axially located single probe in the 0.108 m bubble in the semi-batch mode. The measured values of heat transfer coefficient for the air-water-magnetite system as a function of air velocity, particle size, and solids concentration in the slurry are reported here through typical plots of Figs. 4.34A-F. A critical examination of these figures lead to the following general conclusions.

(a) A comparison of the heat transfer coefficient values for the two-phase (air-water) and the three-phase (air- water- magnetite) systems is interesting in as much as the latter values are greater than the former values at the same air velocity. The differences in the two sets of values are relatively more pronounced at higher air velocities. For air velocities less than 0.08 m/s, the deviations are usually within 3 percent, while for larger air velocities the deviations are usually in the range 5 to 7 percent, except for the case 90.5 μm particles where it is about 13 percent.

This qualitative trend of heat transfer coefficient values can be well understood on the mechanistic picture of the heat transfer process. It is generally believed, and our experiments on temperature history of a heated element in the dispersion have confirmed, that heat removal from an immersed surface is carried out by the elements of dispersion which visit the heat transfer surface in a periodic fashion. Depending upon the degree of bubbling and/or turbulence in the column, these elements periodically and continuously visit the surface and exchange thermal energy while in contact with the heated surface. The amount of energy removed depends upon the properties and residence time of these elements at the surface. From the three-phase system, these dispersion elements have magnetite particles which by virtue of their large thermal conductivity (70 W/m K) in comparison to air (0.026 W/m K) and water (0.6 W/m K), and large

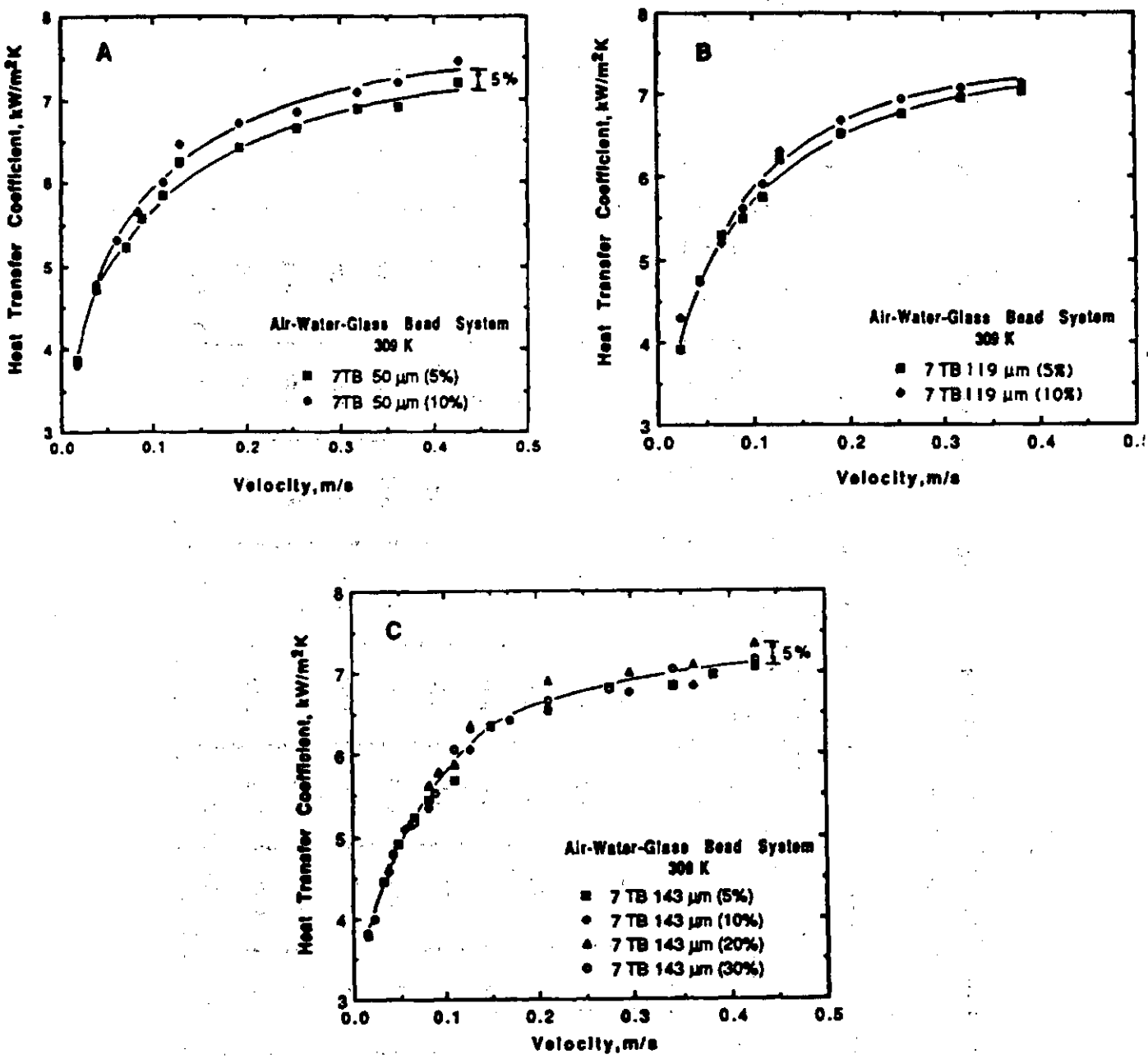

Fig. 4.32. Influence of slurry concentration on heat transfer coefficient for particles of mean diameter (A) 50 μm, (B) 119 μm, and (C) 143 μm.

Table 4.19. Smoothed h_W (kW/m^2K) values for air-water-glass bead system at 309K. Column diameter: 0.108 m, Internals: 19 mm single tube and seven-tube bundle.

Air Velocity (m/s)	Air-Water		Air-Water-Glass Beads (10Wt%)						Air-Water-Glass Beads (10Wt%)		
			50 μm		119 μm		143 μm		h_w(1T)		h_w(0 T)
	h_w(1T)	h_w(0 T)	h_w(1T)	h_w(0 T)	h_w(1T)	h_w(0 T)	h_w(1T)	h_w(0 T)	50 μm	119,143 μm	50,119,143 μm
0.02	3.50	3.80	3.94	4.03	4.20	4.20	4.00	3.95	3.90	4.00	4.05
0.04	4.45	4.68	4.40	4.85	4.75	4.75	4.90	4.72	4.40	4.80	4.78
0.08	5.25	5.43	4.95	5.62	5.45	5.50	5.60	5.50	4.96	5.50	5.55
0.12	5.60	5.89	5.35	6.15	5.90	6.03	6.02	6.00	5.37	5.94	6.02
0.16	5.83	6.19	5.65	6.50	6.24	6.43	6.30	6.30	5.67	6.26	6.35
0.20	6.00	6.41	5.87	6.74	6.50	6.70	6.52	6.50	5.90	6.50	6.60
0.24	6.13	6.58	6.05	6.90	6.67	6.87	6.70	6.65	6.07	6.68	6.80
0.28	6.22	6.70	6.20	7.02	6.82	7.00	6.80	6.75	6.21	6.83	6.92
0.32	6.30	6.80	6.32	7.10	6.94	7.08	6.88	6.80	6.32	6.95	7.04
0.36	6.33	6.88	6.40	7.16	7.00	7.12	6.94	6.85	6.41	7.03	7.10
0.40	6.38	6.94	6.48	7.20	7.08	7.18	6.98	6.88	6.50	7.10	7.15

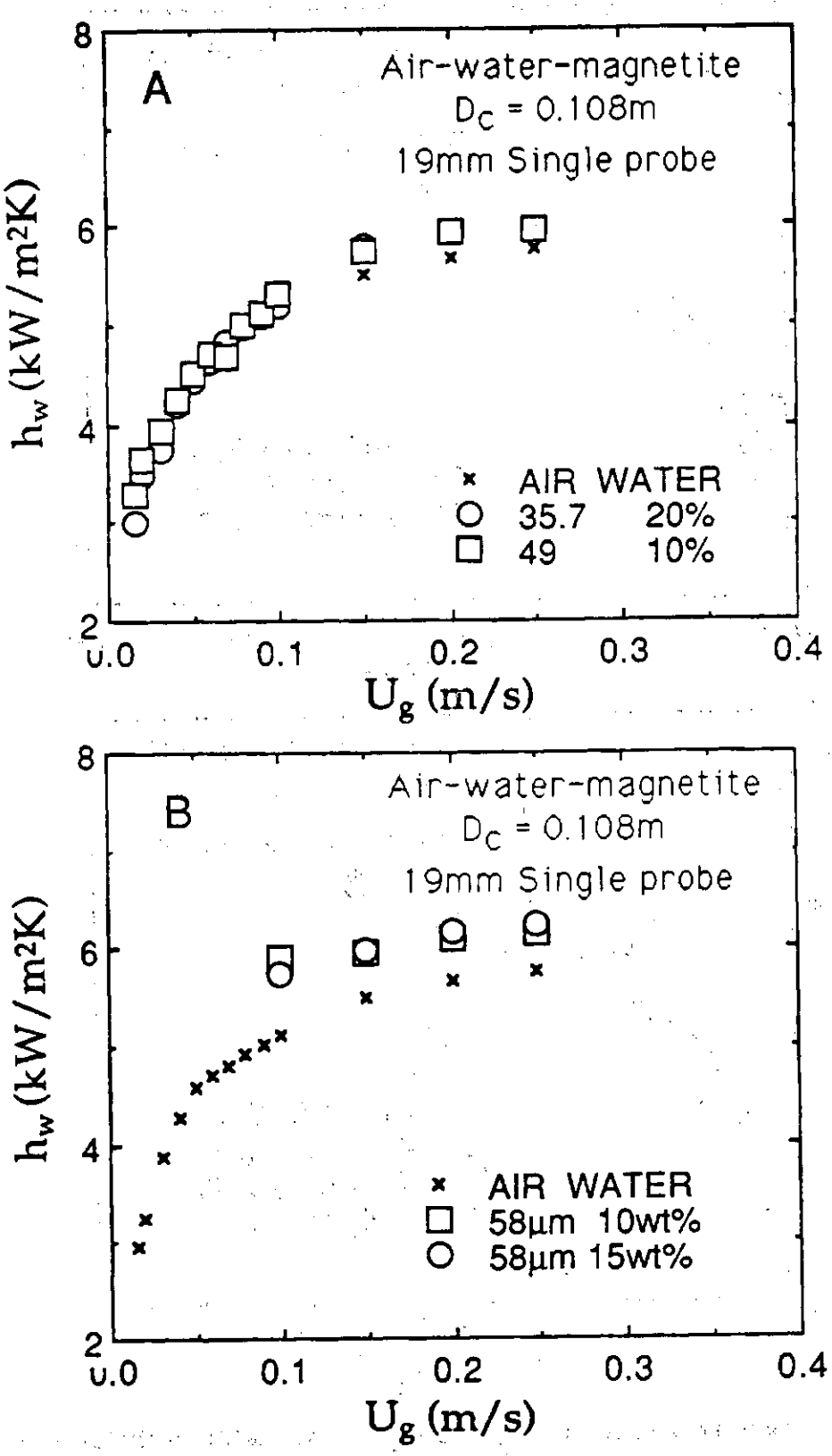

Fig. 4.34. Dependence of h_w on U_g and w_s for magnetite particles of different sizes.

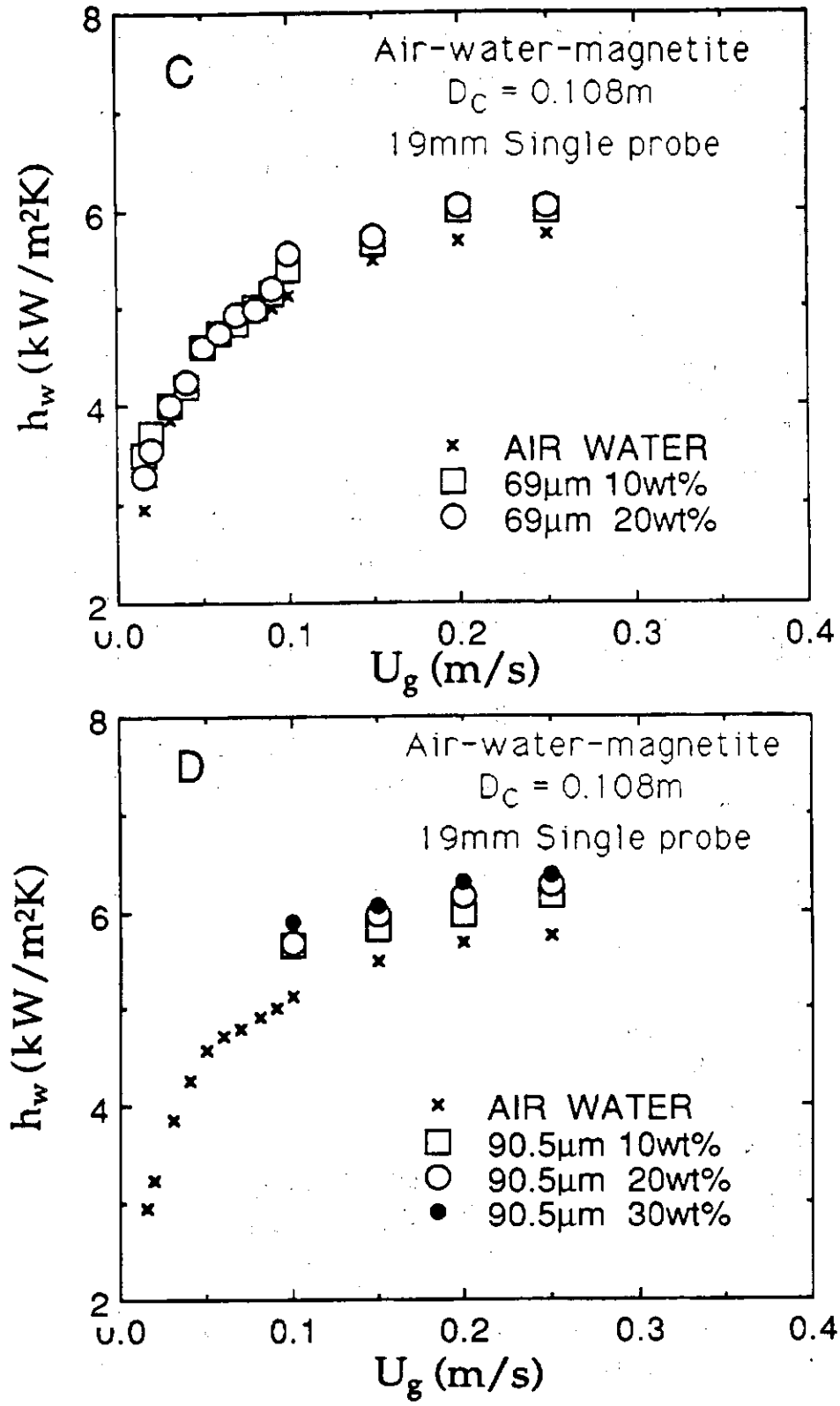

Fig. 4.34. Dependence of h_w on U_g and w_s for magnetite particles of different sizes.

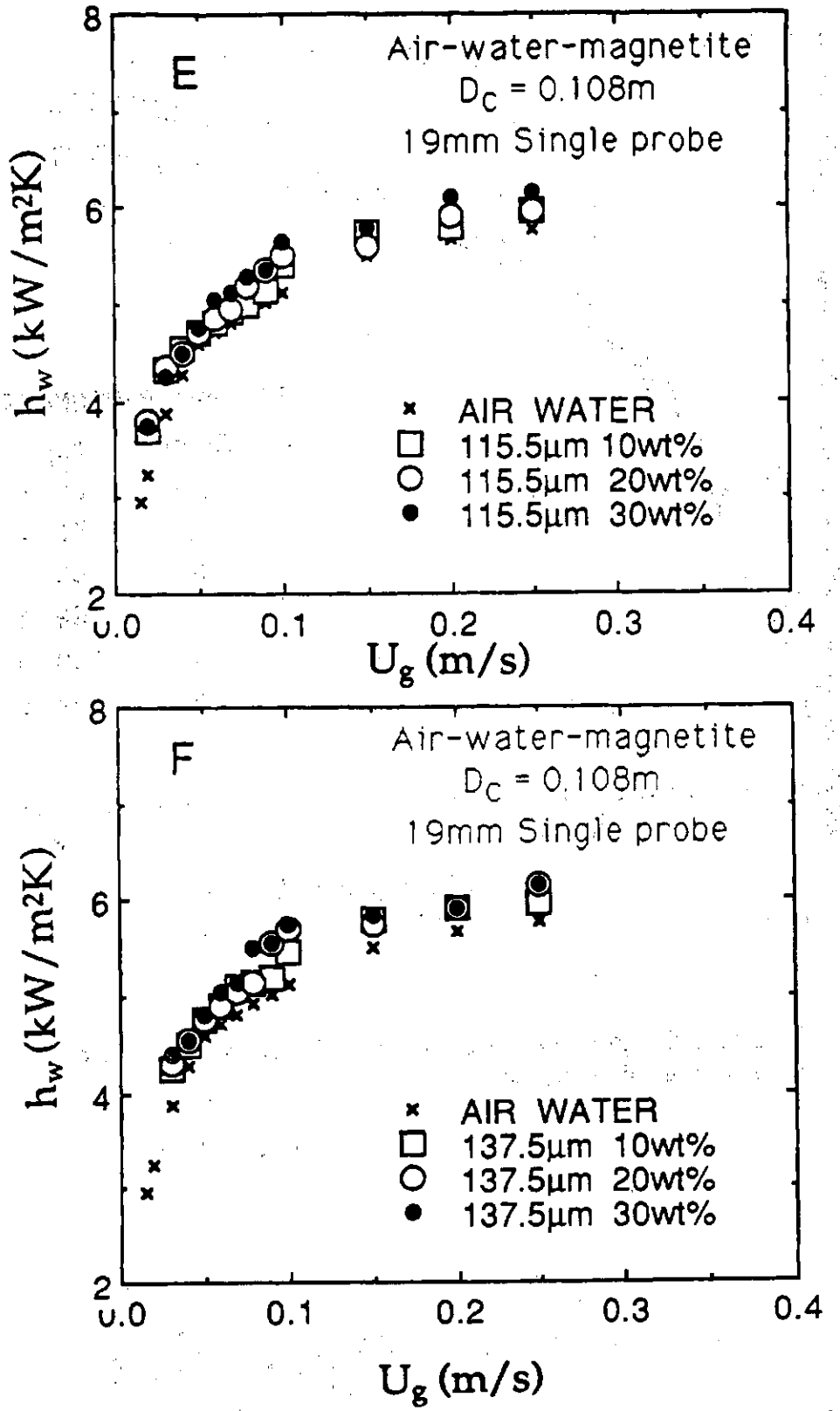

Fig. 4.34. Dependence of h_w on U_g and w_s for magnetite particles of different sizes.

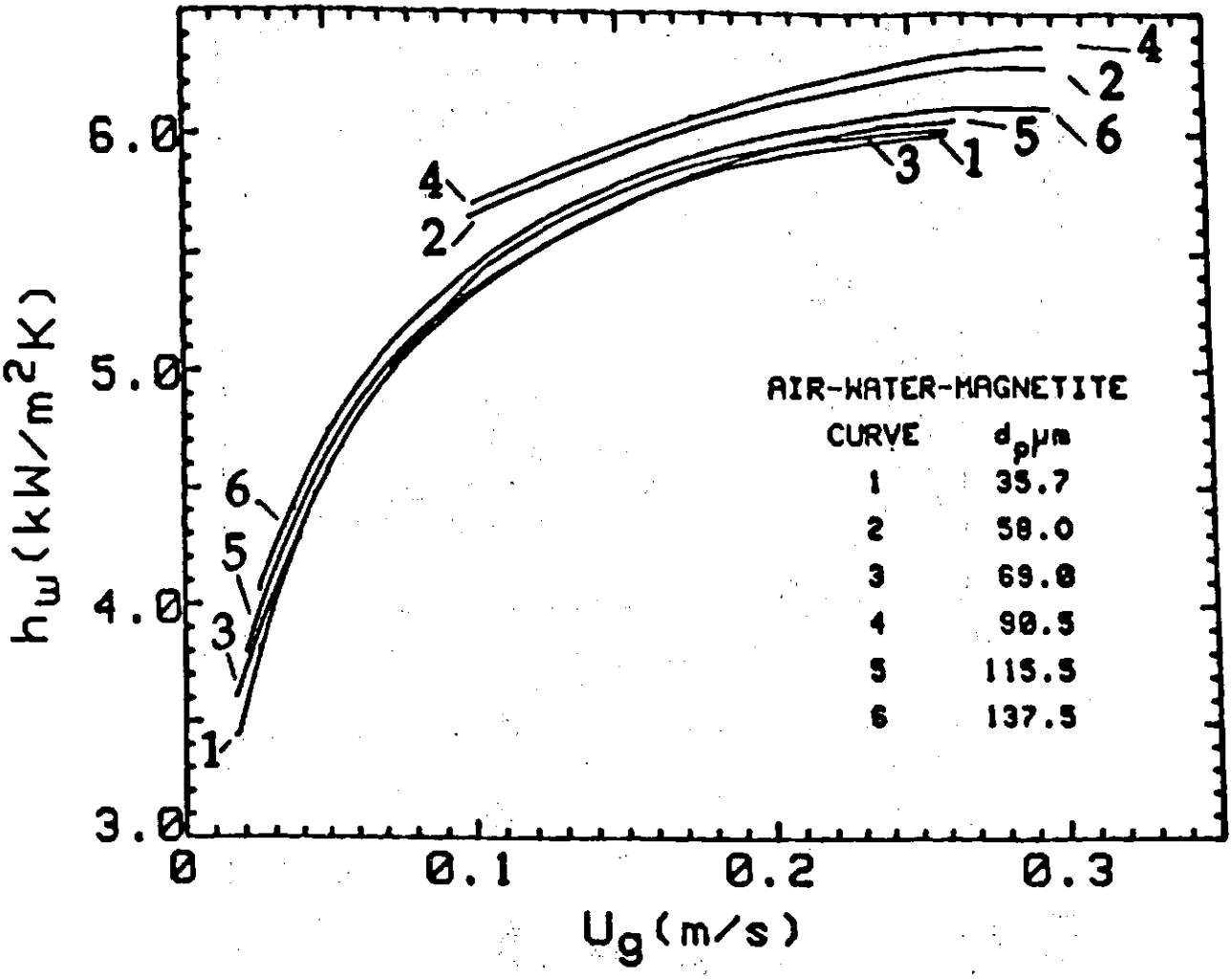

Fig. 4.35. Dependence of heat transfer coefficient on particle diameter in the slurry as a function of air velocity.

volumetric heat capacity are relatively more efficient in removing thermal energy at a faster rate. Note that this process is even augmented by the composition of the liquid elements in three-phase systems as for such systems the air holdup is smaller than for the corresponding two-phase system (gas-liquid only) at the same air velocity, as discussed above. The smaller holdup implies relatively larger bubbles in the column and these could create more turbulence and hence shorter residence time of the liquid elements at the heater surface. as a result the heat transfer coefficient will increase.

(b) Figures 4.34B-E portray the influence of slurry concentration on heat transfer coefficient for a given particle size as a function of air velocity. It appears that the effect of slurry concentration on heat transfer coefficient is particle size dependent, and it is more for larger particles. For slurries containing particles smaller than about 100 μm, the effect of slurry concentration is small for the range investigated here and no systematic trend is obvious. The heat transfer coefficient values may be represented by an average curve having a deviation of less than $\pm$ 3 percent. For slurries of particles greater than 100 μm, the heat transfer coefficient initially increases with the increase in solids concentration (10 to 20 weight percent) but thereafter further increase (20 to 30 weight percent) produces only negligible increase in the heat transfer coefficient values. Usually, this increase in heat transfer coefficient with the initial increase in solids concentration is more at higher gas velocities and decreases with decrease in gas velocity.

This small influence in solids concentration in the slurry on heat transfer coefficient can be explained on the basis that increases in solids concentration in the dispersion element does not significantly alter and improve the efficiency of heat transfer. The heat transfer rate process is determined by the relative contributions of two competing processes; viz., the residence time or renewal rate of the dispersion element which alters those physical properties which are basically effective in removing heat. At lower gas velocities, the former has more significance and hence the composition of the element does not alter the heat transfer rates. At higher gas velocities the latter is relatively more important and hence variation in slurry concentration shows a greater influence. However, it appears that the dispersion element properties in general have a smaller

contribution on heat transfer rate after a certain concentration of solid is reached in the dispersion element.

(c) The effect of magnetite particle diameter in slurry on heat transfer rate at a given air velocity is explicitly displayed in Figs. 4.34A-E, and 4.35. In the latter plot for slurries of different particle sizes, the data referring to either 20 weight percent or to the mean of 20 and 30 weight percent are plotted. A very weak dependence on particle diameter is evident and the maximum variation in the heat transfer coefficient values is about 4 percent for all particles studied here. A more closer examination suggests inconclusive but probable trend that heat transfer rates may increase slightly with increase in slurry particle size. The magnitude is within the range of our experiment error ($\pm$ 4.5 percent) and hence our present effort is incapable of conclusively establishing this small trend which is probably real. The symptom of this trend is present in our data by a small systematic difference in heat transfer coefficient values when slurries of different particles sizes are studied in a consecutive order. The smoothed h_w data values for a given d_p and C_s are given in Table 4.9.

The experimental data and the observed trends as explained above point to the fact that the mechanism of heat removal is by the elements of dispersion which periodically visit the heat transfer surface. The role of solid particles in the dispersion element though not insignificant in influencing the heat transfer rates, is also found to be only of secondary importance. This conclusion is based on the observed effect of solids concentration and particle size on heat transfer rates. This would also suggest that the heat transfer process is not by direct participation of the solid particles but only through a dispersion element which is composed of all the three phases present in the column. It is, therefore, inferred to develop a mechanistic theory of heat transfer from an immersed surface in a slurry bubble column along this line by defining as best as possible the likely changes of this element properties with changes in the properties of the three phases.

The heat transfer coefficient data [129] corresponding to seven-tube bundle and slurry concentrations of 10 and 30 weight percent are shown in Fig 4.36. The heat transfer coefficient has a small dependence on the concentration of solids in the slurry. The two-phase data for the air-water system are also shown in this

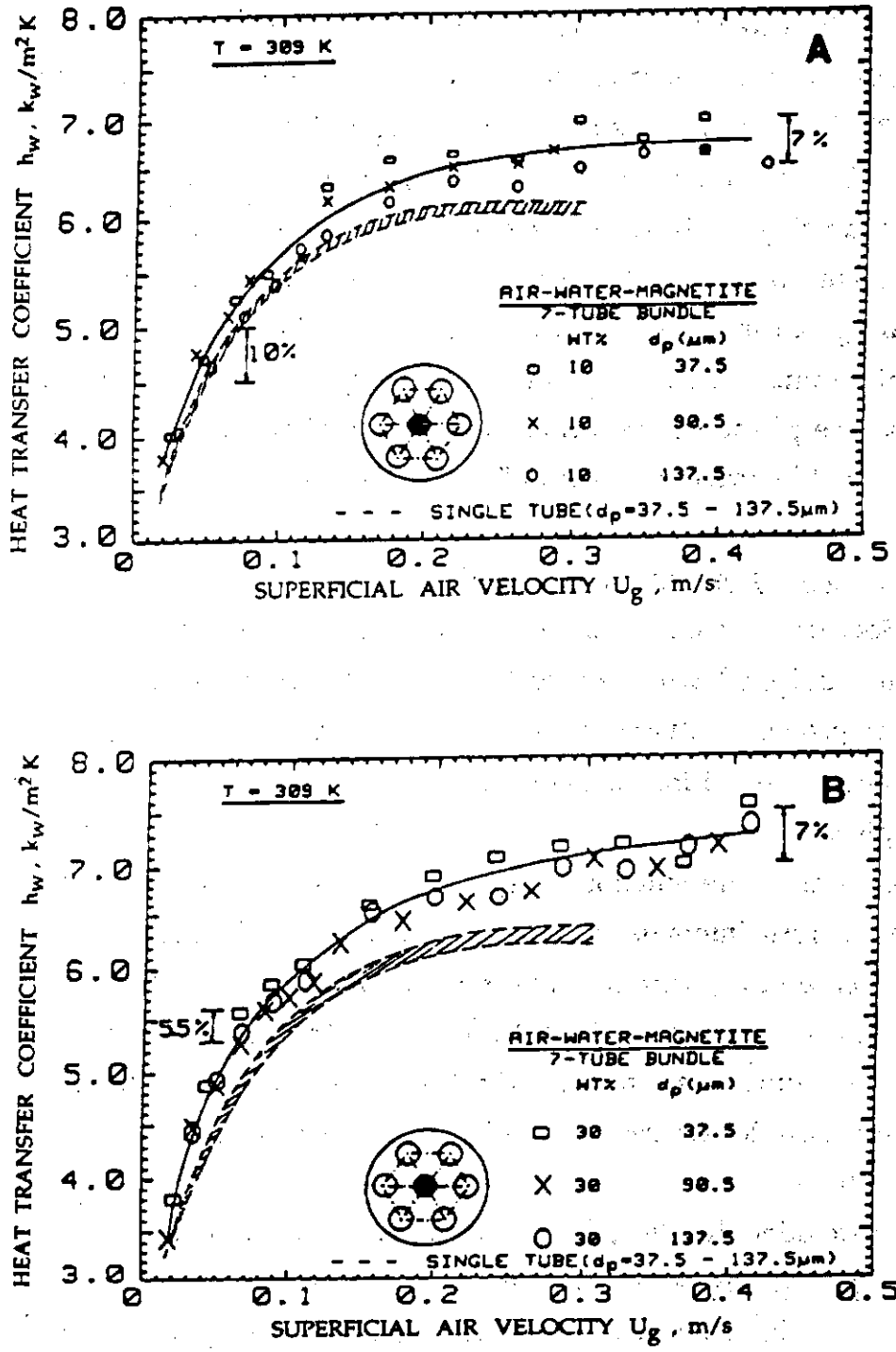

Fig. 4.36. Dependence of heat transfer coefficient on air velocity and particle diameter for slurries of (A) 10 weight percent, and (B) 30 weight percent.

figure. These data collectively interpreted seem to suggest that the heat transfer coefficient decreases slightly as the concentration of solids in the slurry is increased. The influence of slurry concentration is more explicitly displayed in Fig. 4.37. In both cases we find that the dependence on particle diameter is weak, if any. The continuous curve represents the mean values. Also shown in these figures are single tube data which are also independent of particle diameter. The shaded area represents the scatter of the data. The recommended experimental data are given in Table 4.20. The single tube data are systematically smaller than the tube bundle data. A quantitative interpretation of h_w in terms of bubble coalescence phenomenon including entrance effect, and its role in heat transfer process will be presented later in Section 5.4.

4.4.7 Nitrogen-Therminol-Red Iron Oxide System

Heat transfer studies are conducted in the semi-batch mode in the 0.108 m column equipped with one of the three different single axially located heat transfer probes of diameters 19.0, 31.8 and 50.8 mm or a seven-tube bundle. Therminol, fine red-iron oxide powder (1.7 μm) and nitrogen gas are used as the three phases.

A detailed presentation of h_w in Fig. 4.38 shows its dependence on U_g and C_s for the four internals. The h_w values, in all cases, increase with U_g and C_s. The increase in h_w with increase in U_g is rapid for $U_g < 0.1$ m/s and h_w attains almost a constant value at $U_g > 0.2$ m/s. The influence of C_s on h_w is nominal at lower concentration, but is significant in some processes since higher concentration levels result in higher conversion levels in an actual plant operation.

To examine the effect of the nature on h_w, the data for 50 wt% are shown in a cross plot in Fig. 4.39. The dependence of h_w on the geometry of internals appears to be somewhat involved and the results are similar to their corresponding two-phase data shown in Fig. 4.25 and Table 4.21. The marked dependence of h_w on the size of internals (h_w for 19 mm is greater than 50.8 or seven-tube bundle) is attributed to the existing liquid circulation pattern which is restricted in case of larger size internals.

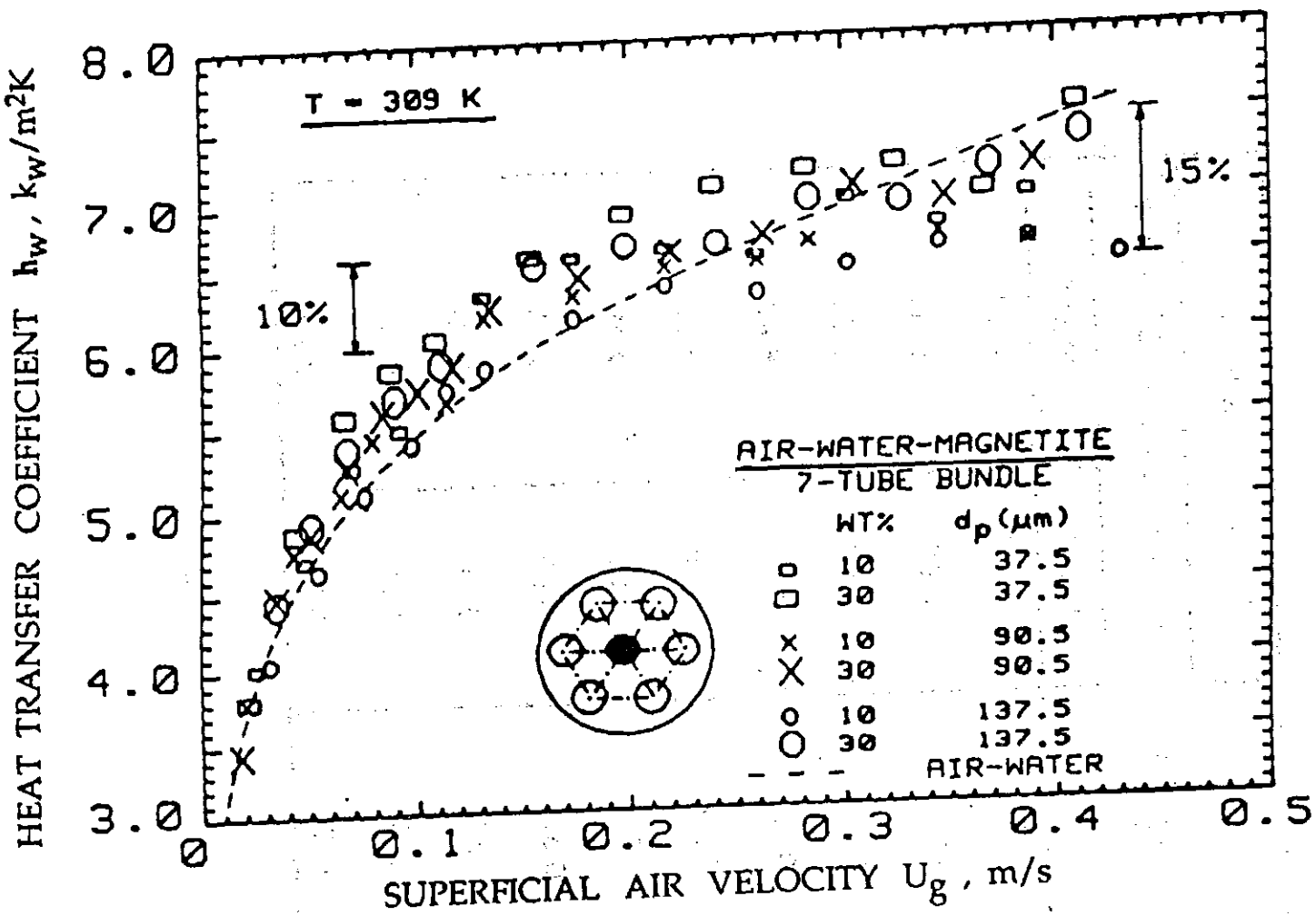

Fig. 4.37. Dependence of heat transfer coefficient on air velocity, particle diameter and slurry concentration.

Table 4.20. Smoothed h_w (kW/m²K) values for air-water-magnetite system at 309K. Column diameter: 0.108m, Internal: Seven-tube bundle.

U_g (m/s)	h_w (kW/m²K)	
	All Sizes 37.5, 90.5, 137.5 μm	
	10wt%	30wt%
0.025	3.80	4.10
0.05	4.65	5.00
0.10	5.60	5.90
0.15	6.15	6.40
0.20	6.45	6.80
0.25	6.55	7.05
0.30	6.65	7.10
0.35	6.70	7.15
0.40	6.65	7.10
0.45	6.60	7.20

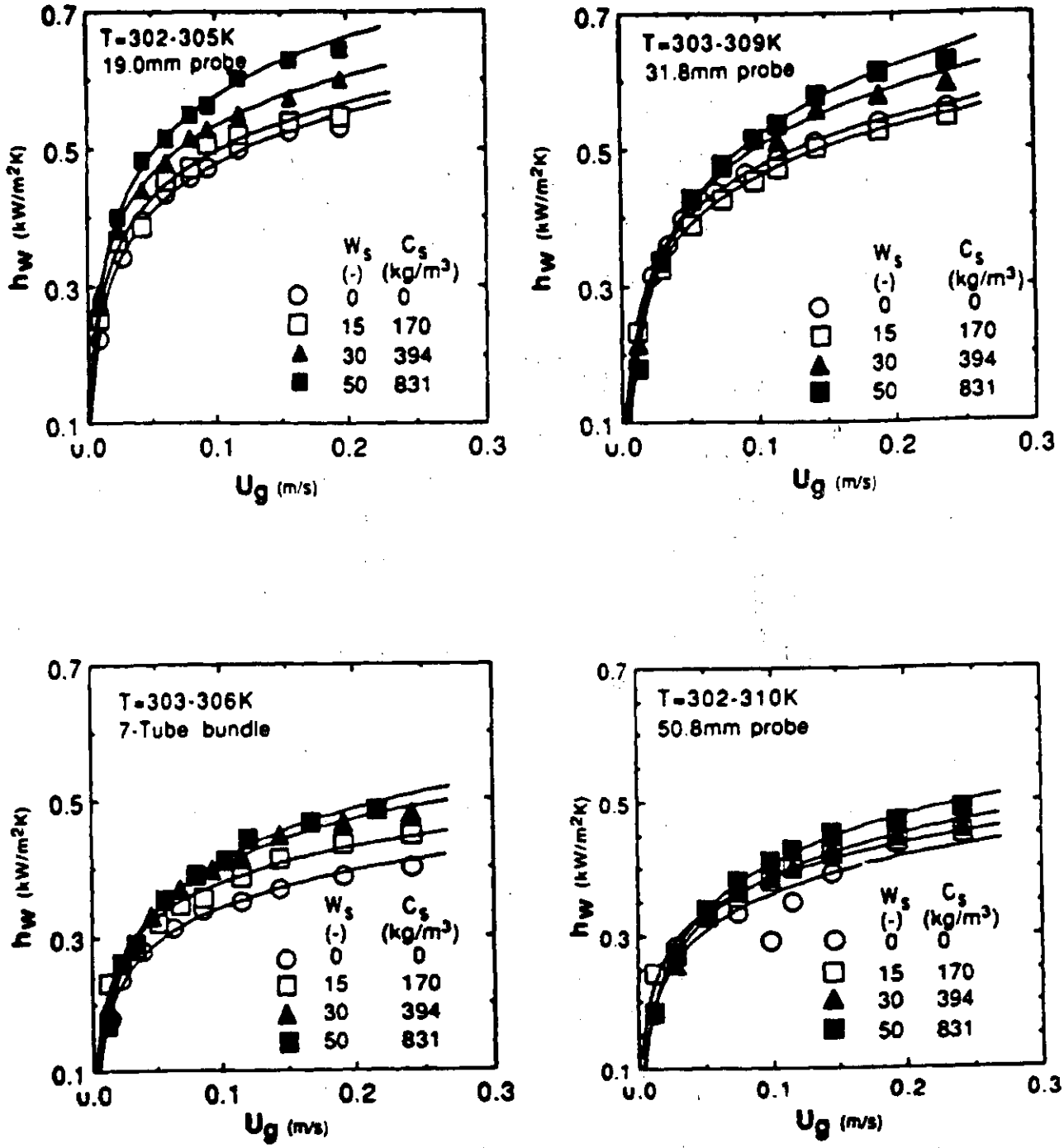

Fig. 4.38. Dependence of heat transfer coefficient for nitrogen-Therminol-red iron oxide on nitrogen velocity and slurry concentration as determined in a bubble column equipped with heat transfer probes of different diameters and a seven-tube bundle.

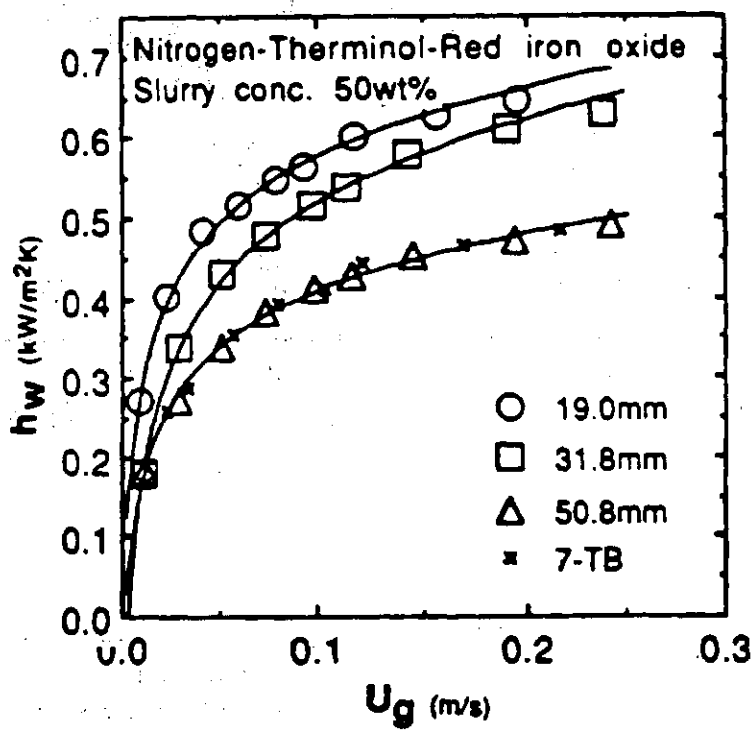

Fig. 4.39. Dependence of h_W on the nature of internals.

Table 4.21. Smoothed h_w (kW/m^{2}K) values for nitrogen-Therminol-red iron oxide system at 301-309K. Column diameter: 0.108 m, Internals: 19.0, 31.8, 50.8 mm single tubes and seven-tube bundle.

U_g	0%	15%	30%	50%	0%	15%	30%	50%	0%	15%	30%	50%	0%	15%	30%	50%
(m/s)	19.0 mm probe				31.8 mm probe				50.8 mm probe				7 - Tube bundle			
0.025	0.340	0.360	0.400	0.410	0.320	0.330	0.335	0.340	0.250	0.255	0.260	0.280	0.240	0.260	0.262	0.265
0.050	0.410	0.430	0.462	0.490	0.390	0.405	0.420	0.425	0.310	0.325	0.340	0.345	0.290	0.328	0.338	0.340
0.075	0.450	0.470	0.510	0.540	0.430	0.448	0.465	0.475	0.340	0.365	0.370	0.380	0.322	0.360	0.380	0.382
0.100	0.480	0.500	0.535	0.580	0.462	0.475	0.502	0.520	0.362	0.382	0.384	0.410	0.340	0.380	0.400	0.412
0.125	0.502	0.520	0.560	0.605	0.485	0.500	0.532	0.550	0.380	0.402	0.410	0.430	0.360	0.398	0.430	0.440
0.150	0.520	0.540	0.575	0.625	0.502	0.515	0.555	0.580	0.400	0.420	0.432	0.452	0.375	0.410	0.445	0.460
0.175	0.540	0.555	0.592	0.648	0.520	0.535	0.572	0.602	0.420	0.440	0.455	0.480	0.380	0.422	0.460	0.475
0.200	0.550	0.568	0.603	0.662	0.532	0.548	0.590	0.622	0.430	0.450	0.462	0.490	0.398	0.435	0.470	0.490